

Digitized by the Internet Archive  
in 2012 with funding from  
LYRASIS Members and Sloan Foundation

<http://archive.org/details/experimentaldete00reyn>



EXPERIMENTAL DETERMINATION OF GAMMA-RAY RESPONSE  
FUNCTIONS FOR THE KSU SPECTROMETER SYSTEM

by 45

ROGER S. REYNOLDS  
B. S., University of Nevada, 1965

---

A MASTER'S THESIS

submitted in partial fulfillment of the  
requirements for the degree

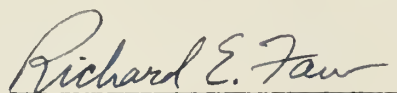
MASTER OF SCIENCE

Department of Nuclear Engineering

KANSAS STATE UNIVERSITY  
Manhattan, Kansas

1969

Approved by:



Major Professor

2668  
74  
1969  
84

TABLE OF CONTENTS

	<u>page</u>
NOMENCLATURE. . . . .	iii
LIST OF FIGURES . . . . .	vi
LIST OF TABLES. . . . .	viii
1.0 INTRODUCTION . . . . .	1
2.0 THEORY . . . . .	3
2.1 Detection . . . . .	3
2.2 Photopeak Parameters. . . . .	10
2.3 Spectrum Analysis . . . . .	15
2.4 Simulation of Infinite Plane Sources Using Point Sources . . . . .	17
3.0 EXPERIMENTAL PROCEDURE . . . . .	22
3.1 Facilities. . . . .	22
3.2 Source Preparation. . . . .	26
3.3 Procedure . . . . .	29
4.0 RESULTS. . . . .	32
4.1 Response Function Normalization . . . . .	32
4.2 Two-Inch Collimator Results . . . . .	32
4.3 Half-Inch Collimator Results. . . . .	39
4.4 Conclusions and Suggestions . . . . .	45
5.0 ACKNOWLEDGMENTS. . . . .	49
6.0 LITERATURE CITED . . . . .	50
7.0 APPENDICES. . . . .	52
7.1 Appendix A: Source Strength Calibration. . . . .	53
7.2 Appendix B: Beta Shield Correction Technique . . . . .	70
7.3 Appendix C: Spectrum Fitting Technique . . . . .	76
7.4 Appendix D: Tabulated Response Functions . . . . .	81

## NOMENCLATURE

<u>Symbol</u>	<u>Explanation</u>
A	Beta shield absorption correction factor
=	
A	Square coefficient matrix used in least squares fit of photopeak
$\bar{B}$	Constants vector used in least squares fit of photopeak
$B_0$	Photopeak width parameter
b(E)	Mean free paths in air from the source plane to the detector
c	Speed of light
$C_1$	Two-inch collimator photopeak response to photons from a point source
$C_2$	Half-inch collimator photopeak response to photons from a point source
$\delta$	Zero energy intercept shift
E	Gamma-ray energy
E'	Energy of scattered photon
$E_0$	Energy of source photons
$E_i$	Representative energy of channel i
$\Delta E$	Energy width of one channel
$\epsilon_p(E)$	Photopeak efficiency
$\phi$	Photon scattering angle
$\phi^{uc}$	Uncollided flux at the source plane, $(\text{cm}^2\text{-sec-sr})^{-1}$
$h_0$	Distance from point source to crystal detector
i	Channel number
$m_0$	Electron rest mass
$\mu$	Gamma-ray attenuation coefficient, $(\text{cm})^{-1}$

<u>Symbol</u>	<u>Explanation</u>
$\mu/\rho$	Gamma-ray mass attenuation coefficient, ( $\text{cm}^2/\text{gm}$ )
$N_o$	Absolute point source emission rate
$N_p$	Photopeak area
$N_t$	Total area of pulse-height distribution
$P(E)$	Peak-to-total ratio
$R$	System resolution, percent
$R_1$	Two-inch collimator photopeak response to photons from an infinite plane source
$R_2$	Half-inch collimator photopeak response to photons from an infinite plane source
$r$	Gain shift ratio
$r_o$	Radius of crystal detector
$\bar{S}$	Solution vector for least squares fit of photopeak
$S_A$	Source strength per unit area
$S_R(E)$	Lip penetration and wall scattering correction factor
$\sigma$	Standard deviation
$\sigma_{\text{inc,BS}}^{\text{KN}}$	Klein-Nishina incoherent backscattering cross section
$\frac{d\sigma_c(\theta)}{d\Omega}$	Differential Klein-Nishina Compton scattering cross section
$t_o$	Thickness of crystal detector
$T(E)$	Calculated absolute detection efficiency of the crystal
$\tau(E)$	Gamma-ray absorption cross section
$W_o$	Full width of photopeak at half maximum
$W(x), W_i$	Weighting factor used in least squares fit of photopeak

<u>Symbol</u>	<u>Explanation</u>
$x$	Pulse-height units
$x_0$	Pulse height where maximum count rate in photopeak occurs
$x_i$	Mean pulse height in channel $i$
$\Delta x$	Pulse-height width of one channel
$Y_i$	Count rate in channel $i$
$Y_0$	Maximum count rate in photopeak
$Y(x)$	Pulse-height distribution
$\theta$	Photon scattering angle in differential Klein-Nishina scattering equations

## LIST OF FIGURES

	<u>PAGE</u>
1. Typical pulse-height spectrum. . . . .	4
2. Gamma-ray mass attenuation coefficients for NaI(Tl). . .	6
3. Photomultiplier tube base circuit. . . . .	8
4. Schematic representation of collimator-source plane relationship. . . . .	19
5. Typical photopeak responses as a function of the distance off the detector center line, Mn-54. . . . .	20
6. Machine drawing of the KSU collimator. . . . .	23
7. Block diagram of equipment set-up. . . . .	24
8. Collimator assembly and source rack. . . . .	25
9. Source preparation apparatus. . . . .	28
10. Typical two-inch collimator response function, Zn-65 . .	33
11. Two-inch collimator infinite plane response functions. .	36
12. Photopeak amplitude as a function of energy, two-inch collimator. . . . .	37
13. $B_o$ as a function of energy, two-inch collimator. . . . .	38
14. Percent resolution as a function of energy, two-inch and half-inch collimators. . . . .	42
15. Comparison of two-inch collimator and half-inch collimator photopeak heights . . . . .	43
16. Photopeak response of half-inch collimator system to Ce-139 gamma rays. . . . .	44
17. Source-detector geometry for absolute counting experi- ments. . . . .	54
18. Counting cavity for absolute counting experiments. . . .	58
19. Detector assembly for absolute counting experiments. . .	59
20. Typical spectrum obtained during absolute counting, Hg-203. . . . .	61



21. Illustration of spectrum correction technique. . . . . 62

22. Lip penetration and wall scattering correction factor  
as a function of energy for the two-inch collimator  
response functions. . . . . 68

## LIST OF TABLES

	<u>PAGE</u>
I.        Verification of absolute counting technique. . . . .	64
II.       Source strengths of experimental isotopes. . . . .	69
III.      Total beta shield loss cross sections. . . . .	73
IV.      Comparison of beta shield corrected spectra. . . . .	74

## 1.0 INTRODUCTION

Infinite planes of gamma-ray sources are of interest in fallout radiation studies. The energy distribution of the gamma-ray flux arising from such a source is usually measured using a scintillation spectrometer system consisting of a light-producing crystal, photomultiplier (PM) tube, associated amplifiers and power supplies, and a multichannel pulse-height analyzer. The accumulated pulse-height spectrum represents the response of the system to the gamma rays striking the crystal. The primary information desired from such a spectrum is the energy distribution of the gamma-ray flux at the crystal. In order for such an analysis to be possible, the response of the spectrometer system to photons of known energy and intensity must be measured.

The energy distribution of the incident flux may vary with direction. Consequently, measurements are usually made with a collimated detector, which limits the measurements to a specified direction. It should be noted, however, that the collimator itself influences the system response.

Differences between the true energy distribution and the pulse-height distribution are caused by two types of distortion, detection distortion and electronic distortion. The distortion in the detection is caused by the statistical nature of the gamma-ray interactions in the crystal and the scintillator variance. The electronic distortion is a result of the various staged processes required to convert the light output of the crystal into a voltage pulse, and the subsequent transfer of the voltage pulse from the output of the PM tube to the multichannel analyzer (MCA). If the response of the system to monoenergetic photons is measured, one has in effect measured the distortions associated with photons of that particular energy. Once these measurements are completed for several different photon energies,

the analysis of a complex experimental spectrum reduces to a mathematical problem of determining the set of energies and intensities which best represent the experimental spectrum (3, 15, 12, 4).

Typical problems encountered are the measurement of the angular distribution of barrier-transmitted radiation, or the angular distribution of gamma-ray photons reflected from a barrier. In order to determine the energy distribution of the flux measured in these types of experiments, it is necessary to know the system response to a uniform flux of known energy distribution. The basic requirement is that the flux be constant across the collimator aperture. In order to produce a flux which satisfies this requirement, an infinite plane isotropic source is simulated. The simulation may be accomplished by a point source superposition technique. The use of the KSU collimator-spectrometer system to measure energy and angular distributions, which are to be analyzed using the response functions presented in this work, imposes no geometrical restrictions. The only restriction is that the photon flux must be uniform across the collimator aperture.

This study is concerned with experimentally measuring the response of the Kansas State University spectrometer system to photons from nine monoenergetic gamma-ray emitters, i.e., Pb-210 (47 keV), Cd-109 (88 keV), Ce-139 (166 keV), Hg-203 (279 keV), In-Sn-113 (392 keV), Sr-85 (513 keV), Cs-Ba-137 (662 keV), Mn-54 (840 keV), and Zn-65 (1114 keV).

## 2.0 THEORY

### 2.1 Detection

The response of the spectrometer system is primarily a function of the detection process. The system under consideration employs a NaI(Tl) scintillator crystal connected to a ten stage PM tube. The height of the voltage pulse at the output of the PM tube is proportional to the amount of energy deposited in the crystal detector, (3,17,4). This proportional nature allows the use of a multichannel analyzer which stores the voltage pulses in a magnetic memory unit according to their height; thus the accumulation of a pulse-height spectrum is realized. The observed distribution represents the total response of the system, as arranged, to the gamma radiation being studied. Figure 1 shows a typical response curve for a monoenergetic gamma-ray source with characteristic X ray, indicating the main features of the distribution. The shape of the spectrum is a consequence of the photon interactions in the crystal. The source photons will interact with matter in three principle ways, photoelectric absorption, Compton scattering, or pair production.

In photoelectric absorption the entire energy of the photon is transferred to an electron in one collision. The Compton effect is characterized by the fact that only a portion of the photon energy is transferred to an electron in a collision. The amount of energy lost by the photon is a function of the scattering angle, as shown by equation (2.1), where E and E' are respectively the initial and final photon energies.

$$E' = \frac{E}{1 + \frac{E}{m_0 c^2} (1 - \cos\phi)} \quad . \quad (2.1)$$

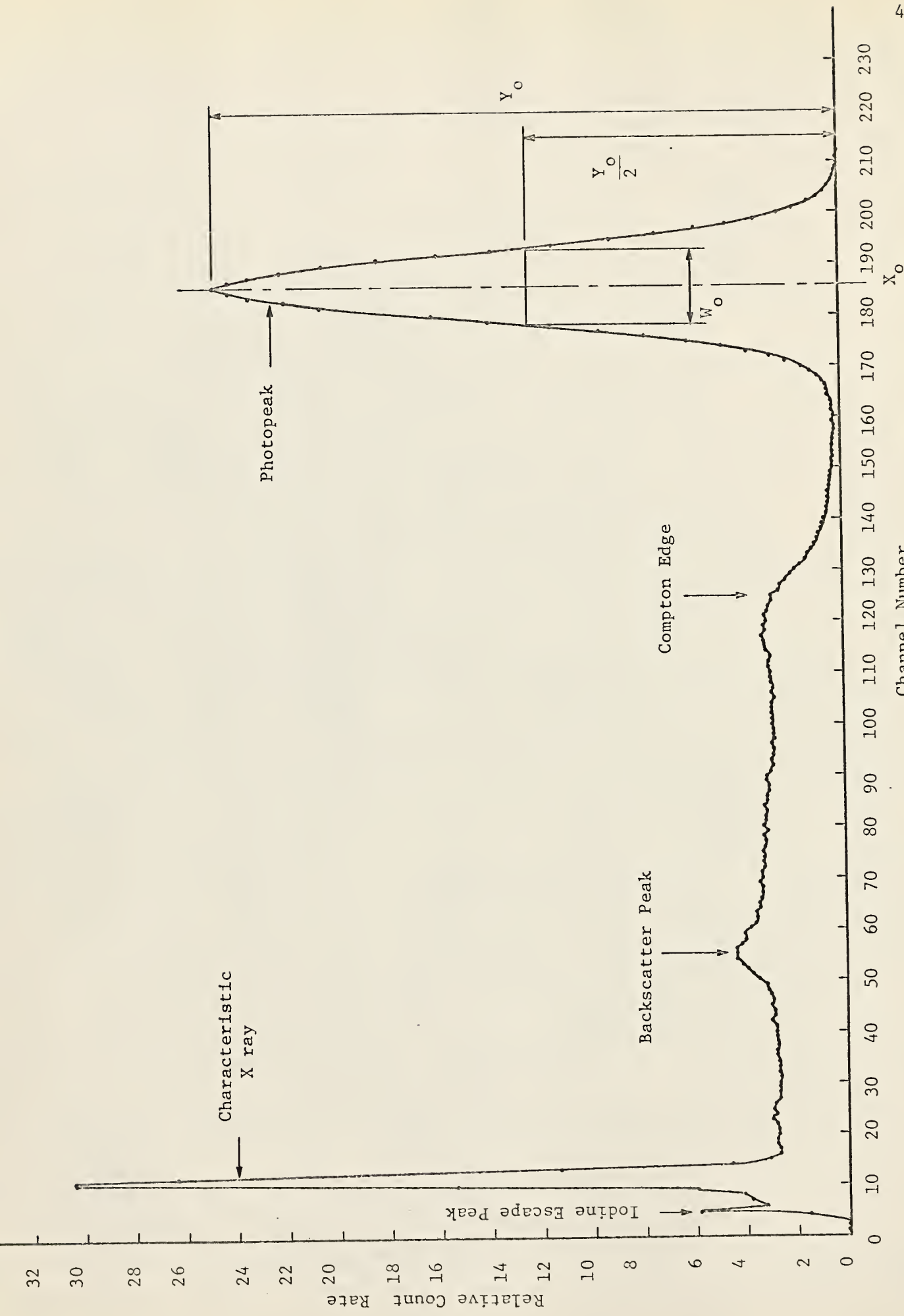


Figure 1. Typical pulse-height spectrum.

The photon exit angle,  $\phi$ , is measured with respect to the incident direction;  $m_0$  is the electron rest mass.

The largest possible energy loss occurs when the photon undergoes a head-on collision with an electron and scatters  $180^\circ$ . The smallest energy loss occurs when  $\phi = 0^\circ$ , i.e.,  $E' = E$ . The Compton distribution begins at zero energy, since the recoil electron has zero energy for  $\phi = 0^\circ$ . The maximum pulse height of the Compton distribution occurs when  $\phi = 180^\circ$ , where the recoil electron has its maximum possible energy. This maximum pulse height is referred to as the Compton edge.

Pair production is a threshold type of interaction between the incident gamma ray and the nuclear forces surrounding the nucleus. A gamma ray may annihilate itself in the nuclear force field and produce a positron-electron pair. The rest mass of each particle is 0.511 MeV, thus the photon must have an energy of at least 1.022 MeV in order to produce the pair. Any excess energy is given to the pair as kinetic energy. The electron and the positron do not travel far from the production point before the positron recombines with an electron and annihilates. The annihilation results in the production of two 0.511 MeV photons traveling in exactly opposite directions. Either or both of these photons may interact in the crystal by Compton or photo absorption mechanisms.

In general it may be said that the lower energy region, below about 300 keV, is dominated by the photoelectric effect. The mid-energy region between 300 keV and 4 MeV is dominated by the Compton effect. At energies much above 4 MeV pair production becomes the dominant effect. These trends are illustrated in Figure 2, which shows the photon interaction cross sections as a function of incident energy, up to about 2 MeV.

NaI(Tl) is a luminescent material. Gamma rays entering the crystal



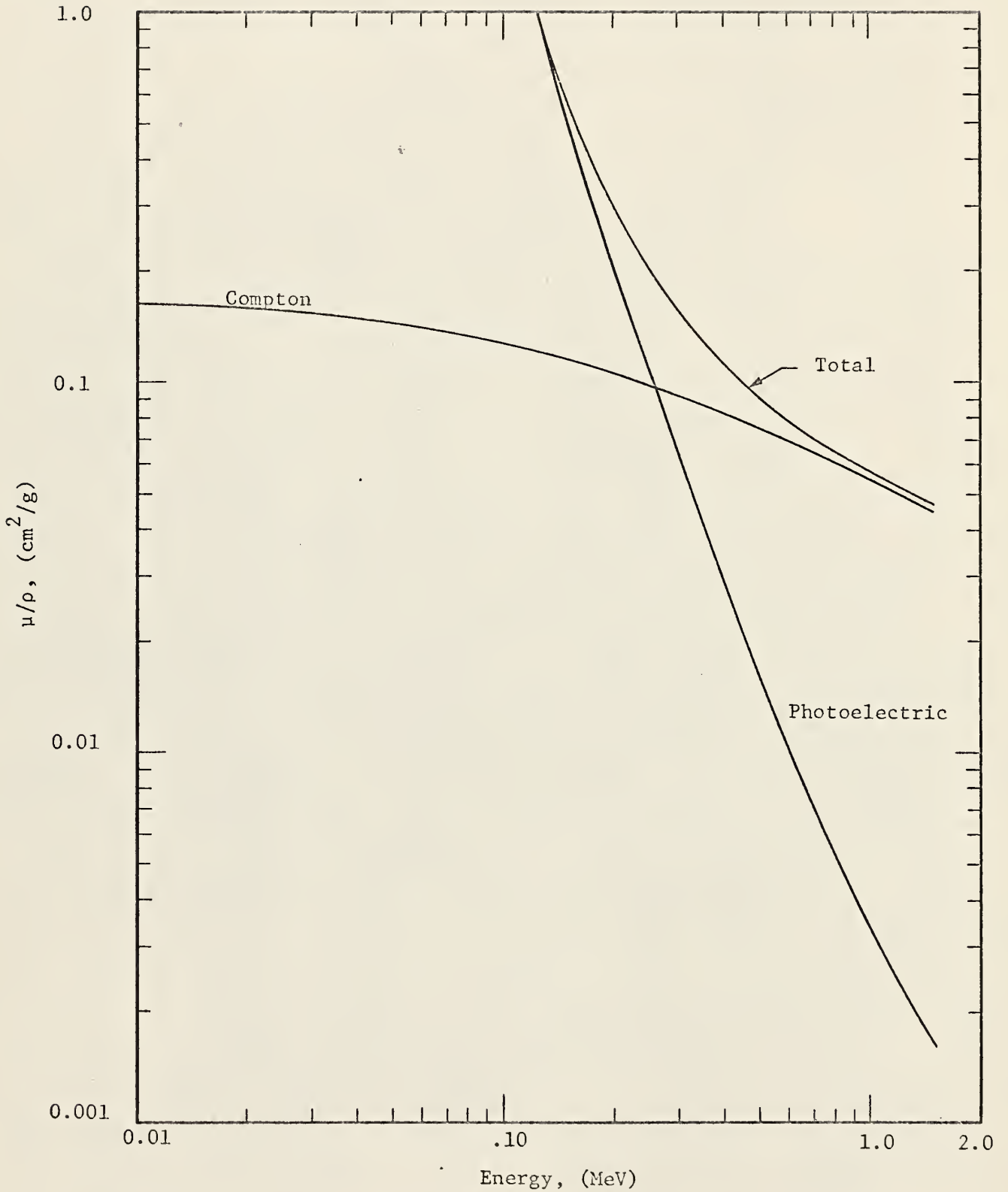


Figure 2. Gamma-ray mass attenuation coefficients for NaI(Tl), from White (21).



detector cause ionization and excitation of the NaI atoms. Reversion to the ground state is accompanied by the emission of visible light. The emission is exponential with a decay constant of about  $3 \times 10^{-7}$  seconds. The crystal is essentially transparent to its own light, which is transmitted through the crystal to the photocathode. The photocathode emits electrons when illuminated by the light. These primary electrons are accelerated in an electric field to a metal dynode which produces secondary electrons when struck by the primary electrons. These secondary electrons are accelerated through another electric potential toward a second dynode where the process is repeated. There are ten such dynodes in the PM tube, and the result after the last stage is an electron multiplication of approximately  $10^7$ . This electron current pulse is then passed through a load resistor, thus producing a voltage pulse across the resistor.

Pulse-height analysis is possible only because the amount of light produced in the crystal is a linear function of the energy deposited in the crystal. The number of primary electrons emitted by the photocathode is proportional to the amount of light striking it. Consequently, the number of electrons directed toward the first dynode is proportional to the amount of energy deposited in the crystal. The electron multiplication through the dynode stages is constant with a stable high voltage power supply. Thus, the number of electrons seen at the collector dynode is still proportional to the amount of energy deposited in the crystal. The current pulse is allowed to pass through a DC blocking capacitor to a load resistor, thus producing a voltage pulse whose magnitude is proportional to the energy deposited in the crystal. Figure 3 is a schematic diagram of the PM tube and the associated tube base electronics used in this study.

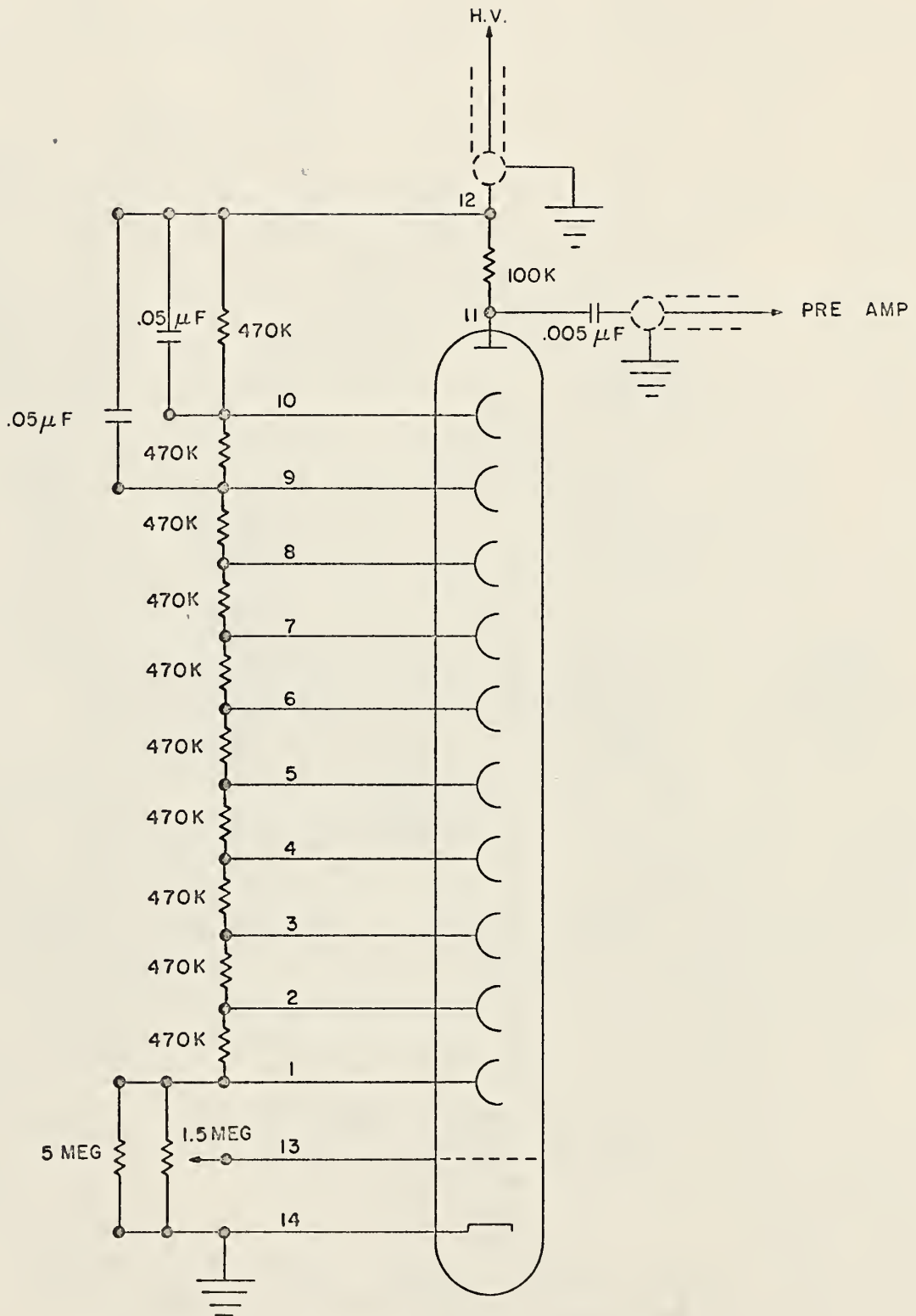


FIGURE 3. PHOTOMULTIPLIER TUBE BASE CIRCUIT.

The photon interactions and the crystal properties form the basis for interpreting the pulse-height distribution accumulated on the MCA. The full energy peak, or photopeak, results when all of the energy of the photon is deposited in the crystal in a time too short to be resolved by the detector. This may be just one photoelectric absorption or a series of Compton scatters followed by a photoelectric absorption.

The Compton distribution extends continuously from zero energy to the Compton edge, since all energies between these limits are possible in the scattering process. The backscatter peak results from photons which initially leave the source in a direction away from the crystal and undergo a large angle scatter, about  $180^\circ$ , and are thus scattered back toward the crystal and subsequently detected. The resulting peak is usually somewhat broad because of the cone of possible backscattering angles realized by the source photons.

The characteristic X-ray peak shown in Figure 1 is not apparent in every gamma-ray spectrum, and is not related to the system response to the monoenergetic photons. Internal conversion processes which may occur in the isotope under study produce X rays which may be detected by the system. These X rays are produced by a source which is independent of the photon source being studied. The X-ray peak must therefore be removed from the response curve associated with the gamma ray. The source photons may, however, excite atoms in the shielding material surrounding the crystal. These excited atoms may undergo internal conversion processes and emit X rays which may be detected by the crystal. These X-ray peaks must remain in the response curve since they are a consequence of the system arrangement. In order to distinguish between these two types of X rays one must have a knowledge of the decay scheme of the isotope under study.

The crystal size will also affect the observed pulse-height distribution. For instance, either one or both of the annihilation photons produced in pair production may escape the crystal without further interaction. If either one of the photons escape, a "one-escape" peak will appear in the distribution just 0.511 MeV below  $E_0$ , the source energy. If both photons escape, a "two-escape" peak will appear in the distribution just 1.022 MeV below  $E_0$ . These escape peaks are a consequence of the fact that all of the source energy, except that which has escaped, has been deposited in the crystal. As the crystal size is increased the probability for escape is reduced because more material is available for the photon to pass through.

Another example of the escape mechanism is the so called iodine escape peak. When a low energy gamma ray or X ray enters the crystal it is usually absorbed very near the surface of the crystal because the interaction probability for absorption is very high for low energies. During the absorption process iodine atoms in the detector are excited and emit 28 keV X rays, which have a high probability for escape since they are produced very near the detector surface. Thus an iodine escape peak appears in the distribution just 28 keV below the associated gamma-ray or X-ray peak.

For a more detailed discussion of the scintillation process, the reader is referred to Price (14).

## 2.2 Photopeak Parameters

In Figure 1 notice that the full energy peak, or photopeak, is approximately Gaussian in shape. In many cases the entire energy of the source photon is not deposited in the crystal in one interaction. Thus, even though the crystal may not be able to resolve the various interactions,

the total amount of light produced in the crystal will vary about some mean value. This mean will correspond to the source energy,  $E_0$ . Another fact basic to the Gaussian shape is the statistical variation in the number of light photons produced by the crystal and the number of photoelectrons produced by the photocathode for a given amount of illumination. Again, the number of photons and photoelectrons produced will vary about some mean value.

It has been said that the amount of light produced in the crystal is proportional to the amount of energy deposited. This is not true in the strictest sense, since below about 72 keV the crystal response is not linear (13). It may happen that zero response occurs at some finite energy. This non-linearity causes the crystal to "add-up" rapidly successive events inaccurately; i.e., events occurring below 72 keV do not produce a proportional response. Consequently, the resulting current pulse produces a voltage pulse which may be higher or lower than the "proportional" height. It has been observed (13) that NaI(Tl) produces higher pulse heights than expected for multiple events. This non-linearity is another reason why the photopeak is other than a spike.

Finally, the source photons may undergo small angle scatters in air or other materials surrounding the detector. These glancing collisions reduce the energy of the photons somewhat before they enter the crystal, and therefore contribute to increased counts on the lower energy side of the photopeak. Since gamma rays do not gain energy in scattering, only the lower energy side of the peak is affected and the distribution is not exactly symmetric, although in most cases the asymmetry is not noticeable.

As previously noted, the data are accumulated on a multichannel differential pulse-height analyzer (MCA). The baseline control is set such



that zero energy corresponds approximately to channel one. The gain control is set such that the energy range of the MCA extends beyond the source photon energy. The accumulated energy spectra are then presented in discrete form as number of counts,  $Y_i$ , in channel  $i$ , where  $i = 1, 2, \dots, 400$ . The data are thus represented as a histogram. The histogram displays the count rate as a function of pulse height (energy). It is important to remember that each channel in the histogram has a finite energy width,  $\Delta E$ . If channel  $i$  is representative of energy  $E_i$ , then all detected photons with energies between  $E_i \pm \Delta E/2$  are registered in channel  $i$ . Notice that the center of the channel is chosen as representative of all photon energies registered in that channel. In other words, all photons with energies between  $E_i \pm \Delta E/2$ , which are detected, are assumed to have an energy  $E_i$ .

Since the photon interaction cross sections in the crystal are continuous functions of energy, the pulse-height distribution is a continuous function. If  $Y(x)$  represents the pulse-height distribution, where the  $x$  are the pulse-height units, the count rate,  $Y_i$ , in channel  $i$  is given as

$$Y_i = \int_{x_i - \frac{\Delta x}{2}}^{x_i + \frac{\Delta x}{2}} Y(x) dx \quad (2.2)$$

where  $x_i$  is the mean pulse height in channel  $i$ . It is assumed that  $\Delta x$  is sufficiently small such that

$$Y_i \doteq Y(x_i) \Delta x. \quad (2.3)$$

As previously discussed, the photopeak may be represented as a Gaussian function,

$$Y(x) = Y(x_0) \exp\left[-\frac{(x-x_0)^2}{B_0}\right] \quad (2.4)$$

$Y(x_0)$  is the maximum count rate in the photopeak;  $x_0$  is the pulse height at which the maximum occurs; this is not to be confused with a channel number.  $W_0$  is the full width of the photopeak at half maximum (FWHM) as given by

$$W_0 = 2(B_0 \ln 2)^{1/2} \quad (2.5)$$

Equation (2.4) may be used to calculate individual points on a Gaussian distribution by rewriting it as

$$Y(x_i) = Y(x_0) \exp\left[-\frac{(x_i-x_0)^2}{B_0}\right] \quad (2.6)$$

Using the approximation shown in equation (2.3) in conjunction with equation (2.6) the photopeak data may be represented as

$$Y_i \doteq Y_0 \exp\left[-\frac{(x_i-x_0)^2}{B_0}\right] \quad (2.7)$$

where  $Y_0 = \Delta x Y(x_0)$ .

Equation (2.7) is suitable for use in a weighted polynomial least squares analysis if one linearizes the equation by taking the natural logarithm of both sides. The result is an equation of the form

$$ax^2 + bx + c = f(x) \quad (2.8)$$

where,

$$\begin{aligned}
 a &= \frac{-1}{B_0} \\
 b &= \frac{2x_0}{B_0} \\
 c &= \ln Y_0 - \frac{x_0^2}{B_0} .
 \end{aligned} \tag{2.9}$$

Solving equation (2.8) for a, b, and c will yield the desired fitting parameters  $x_0$ ,  $Y_0$ , and  $B_0$  after some simple manipulations.

The data in each channel will vary statistically, and it is assumed that the statistical distribution function of each channel is Gaussian. The weighting factors used in the least squares analysis are then given as the inverse of the variance of  $f(x)$ , where  $f(x) = \ln Y(x)$ . Standard propagation of error techniques, as discussed by Beers (2), yield the weighting factor in the log domain as:

$$W(x) = Y(x). \tag{2.10}$$

The pulse-height resolution of the spectrometer system is an overall measure of the system performance (3, 16). The various factors which contribute to the observed resolution are discussed by many authors, (14,3,17,8,4,16) and are only briefly stated here. The factors may be categorized in four main areas, (i) variance in the emission of light photons by the scintillator, (ii) variance in the collection of the light photons by the photocathode, (iii) variance in the emission of electrons from the photocathode and collection at the first dynode, and (iv) variance in the electron multiplication process through the dynode stages. All of these factors are statistical in nature and may be represented mathematically (3,4,17). All of these factors operate in a staged process to distort the photopeak response, the result being a Gaussian shape.



$B_o$ , the width parameter, is used to calculate the resolution of the system. Equation (2.5) allows the calculation of  $W_o$ , which may be stated in units of energy or channels.  $x_o$ , the photopeak pulse height, also corresponds to an energy, i.e.,  $E_o$ , the source energy. The system resolution,  $R$ , is then stated as a percent which is calculated as shown in equation (2.11).

$$R = \frac{W_o}{x_o} . \quad (2.11)$$

A perfect detector would display only a spike, with a resolution of zero. In most cases, a resolution of about 7 percent for Cs-137 is considered good for NaI(Tl).

### 2.3 Spectrum Analysis

The first step in the data analysis is the least squares fit of all the raw data to determine the peak pulse height,  $x_o$ , as well as the other basic parameters previously mentioned. Also, composite Co-60-Cs-Ba-137 quality control spectra must be fitted in order to determine the zero energy channel of the calibration spectra. This is a very important step, because without knowledge of where the zero intercept is for the calibration spectra, the data accumulated may well be useless. The quality control spectra are fitted in the same manner as the experimental spectra. In addition, a least squares straight line is computed to relate  $x_o$  and  $E_o$ , thus determining the calibration slope, keV/channel, and hence the zero-energy intercept.

Once  $x_o$  and the zero energy intercept are determined for the calibration spectra, it is necessary to shift the data in a linear manner such that all of the data are adjusted to the same gain and base line settings. A very small gain shift may not change the spectral data appreciably, but

the effect on the spectrum statistics is quite noticeable. Consequently a gain shift of even 0.5 channels must be accounted for (5).

In this study nine different isotopes were used to measure response functions at energies between 46 keV and 1.114 MeV. Several sets of data were taken for each collimator aperture and for each position. The experimental arrangement will be discussed in more detail in the following sections. A total of approximately 750 spectra were obtained over an eight month period. Consequently, all of the spectra required shifting, since gain drifts and shifts do occur daily.

As previously stated, the shifts in the measured spectra are linear because it is assumed that the MCA operates in a linear manner. If  $x_1$  is the photopeak pulse height in the measured spectrum and  $x_2$  is the corresponding pulse height in the adjusted spectrum, the gain shift ratio,  $r$ , may be given by

$$r = \frac{x_2}{x_1} \quad (2.12)$$

assuming that there is no zero energy shift. Since the variables  $x_1$  and  $x_2$  are continuous functions of energy, it is possible to calculate the new count,  $y(x_2)$ , at  $x_2$  as

$$y(x_2) = \frac{y(x_1)}{r} \quad (2.13)$$

The gain shift ratio used maintains the total area under the curve; i.e., the total number of counts remains the same in the two spectra (8).

For the purposes of illustration, assume that two measured pulse-height distributions  $Y(x)$  and  $Y'(x)$ , are available for the same experiment. However, let the two distributions be on different pulse-height scales. Let

$Y(x)$  be represented by  $m$  channels of data and  $Y'(x)$  by  $n$  channels of data, with  $m$  less than  $n$ . Both distributions cover the same energy range, but the channel width for  $Y'(x)$  is smaller than that for  $Y(x)$ . In order to compare the two distributions directly, the channel widths of each must be the same. Since the energy range is the same,  $\frac{n}{m}$  channels in the  $Y'(x)$  distribution must be equivalent to one channel in the  $Y(x)$  distribution.

The shifting ratio,  $r$ , is  $\frac{n}{m}$ . In order to make the pulse-height scales for the two distributions the same,  $Y'(x)$  is divided by  $r$  and the channel numbers for  $Y'(x)$  are multiplied by  $r$ . Even though the pulse-height scales are the same after the shift, the data in the shifted spectrum do not occur at the same pulse heights as the data for  $Y(x)$ . Consequently, an interpolation procedure must be introduced in order to calculate the count rate at the proper pulse heights. The interpolation is accomplished by choosing a data point nearest the proper pulse-height and a point on either side. These three points are used to calculate the constants in a quadratic equation. This equation is then used to calculate the count rate at the required pulse height. The process is repeated  $m$  times until both distributions match over the entire pulse-height range.

To change the zero energy intercept of the measured spectrum as well as the gain, equation (2.12) becomes

$$r = \frac{x_2}{(x_1 - \delta)} \quad (2.14)$$

Where  $\delta$  is the desired shift in the zero energy intercept of the measured spectrum. Equation (2.13) remains unchanged.

#### 2.4 Simulation of Infinite Plane Sources Using Point Sources

Point source spectra were accumulated for sources placed at equally

spaced intervals off the center line of the collimated detector. A schematic diagram of the geometry is shown in Figure 4. For the two-inch diameter collimator the sources were placed at  $1/2''$  intervals out to a radius of  $4\ 1/2''$  to  $5''$ . The intervals were  $1/4''$  out to a radius of  $1''$  to  $1\ 1/4''$  for the one-half inch diameter collimator. The last radius point used was the position at which the count rate in the photopeak was only 2 or 3 counts per minute above background. Thus, effectively, the contribution to the response function out to an infinite distance was measured. Figure 5 is a typical representation of the photopeak amplitude,  $Y_0$ , as a function of the distance off the detector center line. Notice that the amplitude in the last position is very close to zero and that it is at least two orders of magnitude below the count rate measured at the center position.

In order to represent the infinite plane response, the point source data described above must be numerically integrated in order, by superposition, to generate the response function for a disk source of effectively infinite radius. Before the data can be integrated, however, they must be corrected for radioactive decay and background, and shifted so that the photopeaks for one particular isotope all appear at the same pulse height, and also shifted so that all of the spectra have the same zero energy intercept. Finally, each spectrum must be normalized to the experimental isotope source strength. All of these corrections and normalizations are accomplished by a code written for that purpose called SPECDATA.

The numerical integration of the corrected normalized spectra is performed by DISK which utilizes the WATE subroutine (10). WATE uses Simpson's rule for an odd number of integration points and a modified Simpson's rule for an even number of points to construct a list of integration weights for

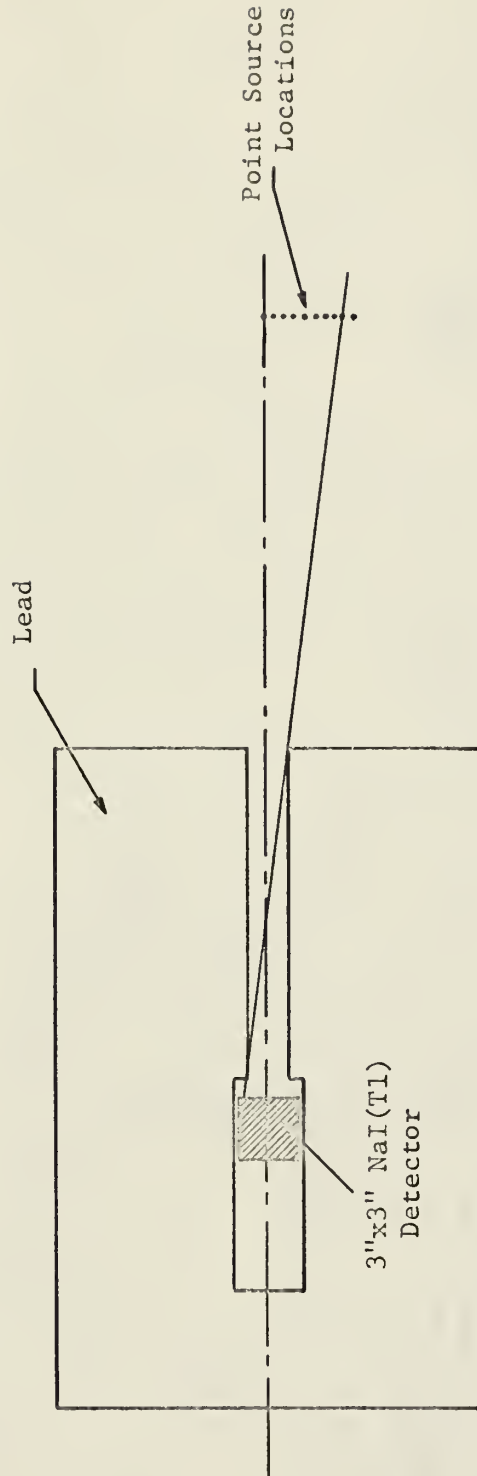


Figure 4. Schematic representation of collimator-source plane relationship.

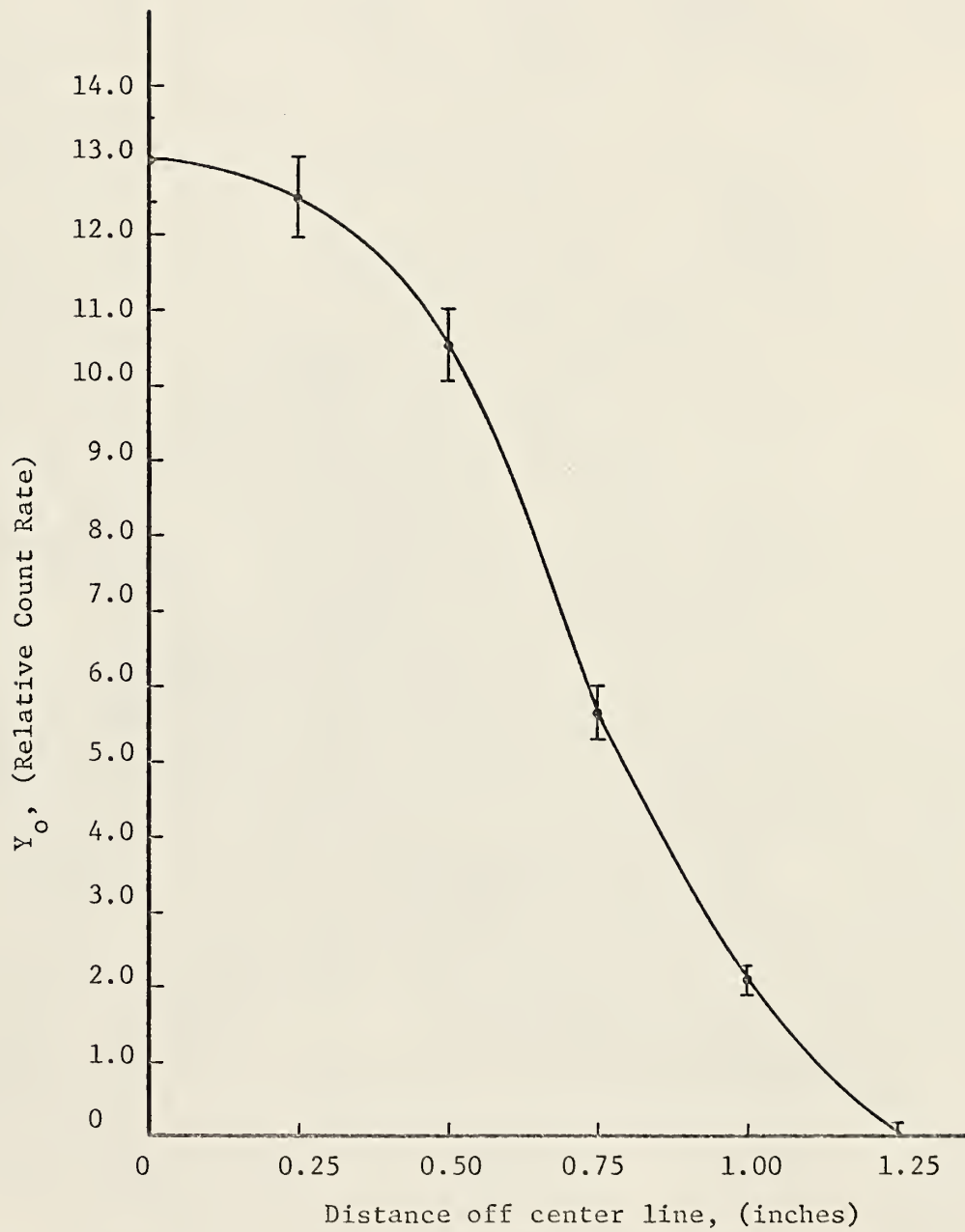


Figure 5. Typical photopeak response as a function of the distance off center, Mn-54, half-inch collimator.



equally spaced data. When only two points are available for the integration, a trapezoidal approximation is applied. Equation (2.15) shows the mathematical scheme used for the numerical integration.

$$\int_0^{2\pi} d\phi \int_0^R f_j(r) r dr \doteq 2\pi \sum_{i=1}^N f_j(r_i) r_i W_i ; j = 1, 2, \dots, 400. \quad (2.15)$$

N is the number of radial points used in the integration, providing N-1 intervals.  $W_i$  are the Simpson integration weights. The integration weights are returned from WATE to MAIN in DISK and the data in each channel of each spectrum are multiplied by the appropriate weight. The multiplied spectra are then added together channel by channel to yield the system response to a radial line source. The system response is azimuthally symmetric, consequently multiplying the line source response by  $2\pi$  yields the system response to a disk source of effectively infinite radius.

After the integration of the data for a particular isotope is completed, the photopeak of the response function is fitted to a Gaussian, for a final check, in order to make sure that the integration process did not change the position of the photopeak appreciably.

### 3.0 EXPERIMENTAL PROCEDURE

#### 3.1 Facilities

The goal of the experiment was to determine the response of the system to gamma rays from an infinite plane monoenergetic source. As previously discussed, the infinite plane was simulated by using point sources in a plane about 100 centimeters from the crystal face. The crystal was placed inside a cylindrical lead collimator. Figure 6 is a machine drawing of the collimator assembly with the appropriate details. Such a device is necessary for many measurements where angular and energy distributions are of interest. The collimator has two degrees of freedom; the base will rotate through  $360^{\circ}$ , while the barrel itself will rotate through  $90^{\circ}$ . There are three collimator plugs available with the assembly, a solid lead blank for use in background measurements, a one-half inch diameter collimator, and a two-inch diameter collimator. The half-inch collimator has an angular resolution of  $1.85^{\circ}$  as measured from the center of the detector face. The two-inch collimator has a resolution of  $7.39^{\circ}$ .

Figure 7 is a block diagram of the experimental arrangement and the equipment used. The infinite plane was simulated by placing the point sources on a wooden rack which was parallel to the collimator face. Figure 8 is a photograph of the collimator assembly and source rack. The meter stick seen on the left was used to measure the source position relative to the center line of the collimator entrance. A plumb bob was hung from the top of the rack such that the plumb bob string intersected the horizontal string at the center of the collimator entrance as projected on the source plane described by the source rack. The center position was checked and calibrated at least twice daily with an optical level to insure reproducibility of the results.



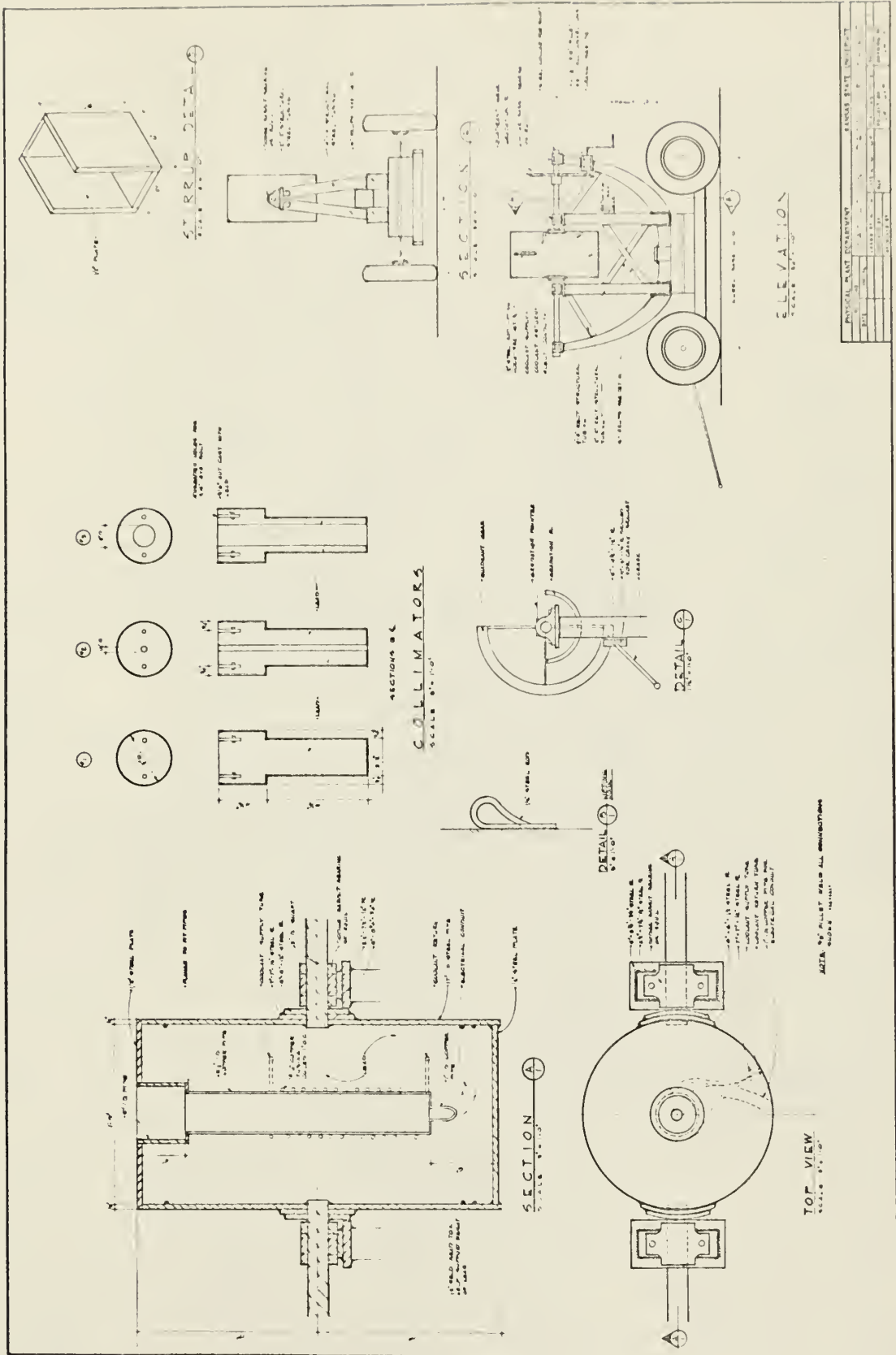


Figure 6. Machine drawing of the KSU collimator.

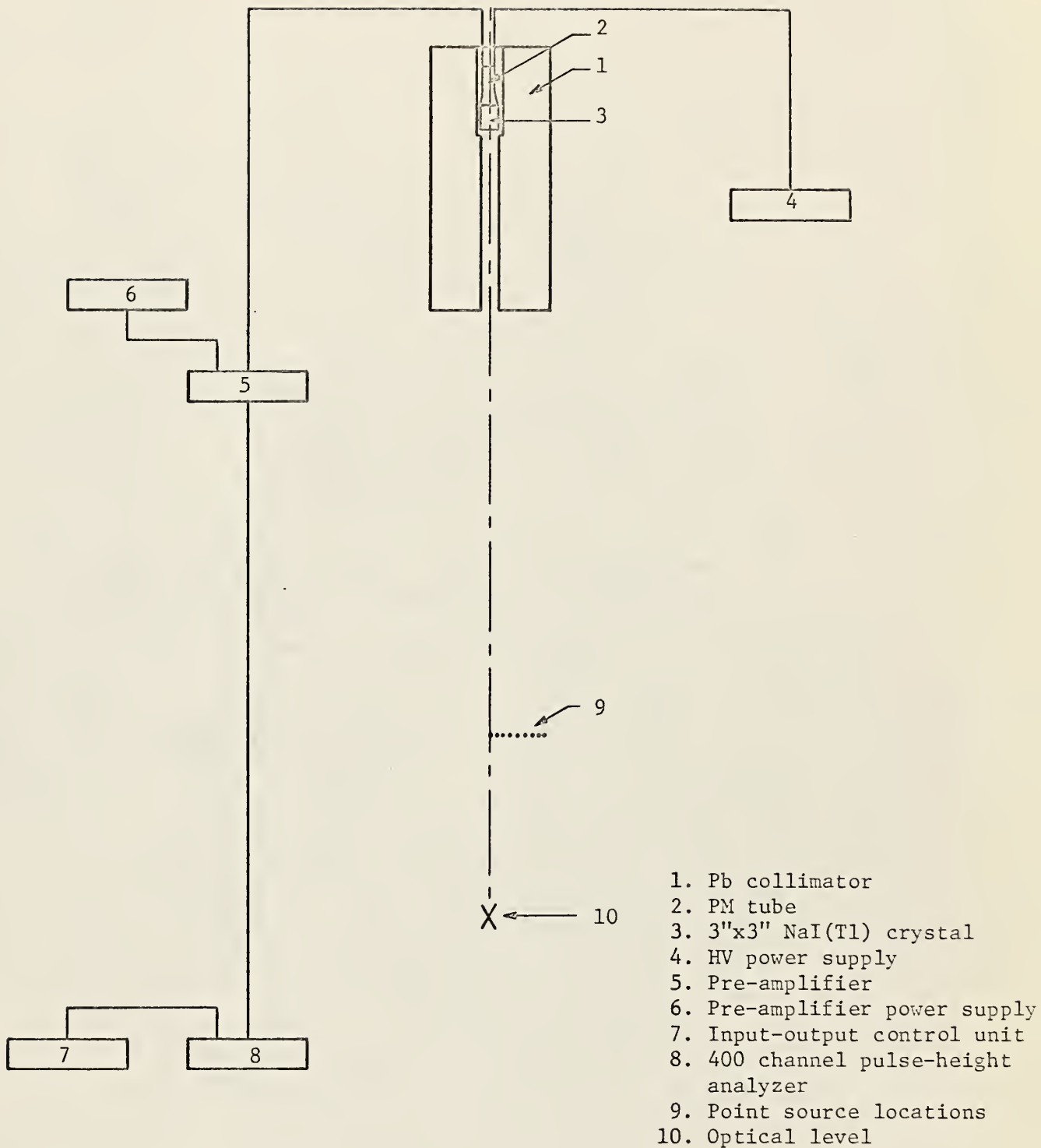


Figure 7. Block diagram of equipment set-up.

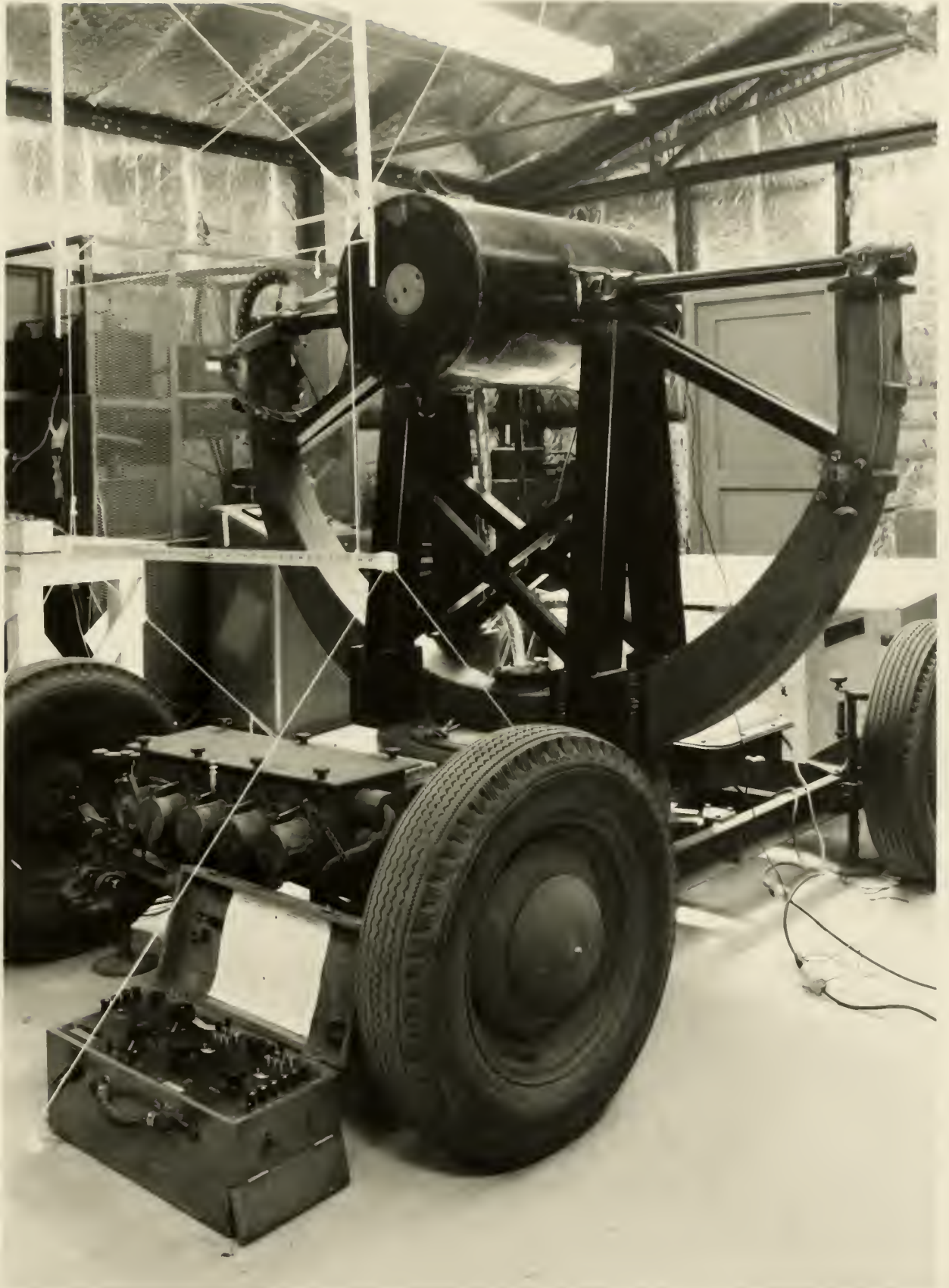


Figure 8. Collimator assembly and source rack.

The potentiometer shown in the lower left of Figure 8 was used in conjunction with a copper-constantan thermocouple to monitor the crystal environment temperature inside the collimator. It is desirable to maintain a constant crystal and PM tube temperature in order to minimize gain drifts and shifts. Also, the thermionic emission current from the dynodes and photocathode should be kept as low as possible. Price (14) indicates that the thermionic current may be reduced by about a factor of two for every ten degree centigrade drop in tube temperature. Since it is not convenient to cool the collimator, it was decided to maintain a temperature as near room temperature as possible inside the collimator. This was accomplished with a constant temperature water bath heater. Heated water was pumped directly into the collimator through copper tubes imbedded in the lead (see Figure 6).

The detector used was a Harshaw Integral Line Assembly, type 12S12, consisting of a 3" x 3" NaI(Tl) crystal, PM tube and associated tube base electronics. The PM tube was powered by a John Fluke, model 412A, high voltage power supply, operated at +1100 Volts. The signal from the PM tube was passed through a Hamner model N-356 cathode follower pre-amplifier, powered by a Kepco model HB2AM voltage regulated power supply operated at +250 Volts. The output of the pre-amplifier was fed through approximately eighty feet of RG-62U signal cable to the input terminal of a TMC model 402-6 400 channel MCA. Output from the MCA was controlled by a TMC model 520 type-punch-read control unit, which permitted read-out by an IBM typewriter or a Tally paper tape perforator, and read-in by a Tally paper tape reader.

### 3.2 Source Preparation

In this study nine isotopes were used as sources for monoenergetic



gamma rays; lead-210 (0.046 MeV), cadmium-109 (0.088 MeV), cerium-139 (0.166 MeV), mercury-203 (0.279 MeV), indium-tin-113 (0.392 MeV), strontium-85 (0.513 MeV), cesium-barium-137 (0.662 MeV), manganese-54 (0.840 MeV), and zinc-65 (1.114 MeV). All of the isotopes were purchased commercially in liquid form and were certified to be 99+ percent pure. Lead-210 was purchased from New England Nuclear Corp., 575 Albany Street, Boston, Mass.; all other isotopes were purchased from Nuclear Science and Engineering Corp., P. O. Box 10901, Pittsburgh, Pa.

Before the sources could be used in the experiments it was necessary to transform them into "point" form. Source mounts were constructed from 1/16" sheets of ordinary plastic and consisted of a 1" O.D., 3/4" I.D. circular section mounted on a two inch long handle to facilitate handling. A thin sheet of transparent mylar film,  $3.5 \text{ mg/cm}^2$ , was sealed to one side of the planchet with Walther's "Goo" (manufactured by Walthers Specialty Inc., Milwaukee, Wisconsin) which was found to give a strong, leak-proof seal. Typically, the planchet weight before loading was about 0.48 grams. The procedure was then to draw the source solution, usually less than 0.1 ml, from the source bottle by means of a micrometer buret (manufactured by RGI Inc., Box 732, Vineland, New Jersey, model S1200A), with a 0.2 ml capacity and 0.0002 ml divisions. Figure 9 shows a typical source bottle, unloaded planchet, and the disassembled buret.

The entire solution was drawn from the source bottle and the volume recorded. The buret tip was then placed above the center of the planchet and clamped into position. Approximately 1/20 of the total volume was placed on the planchet one drop at a time, the buret was then rotated away from the planchet and an infra-red lamp placed in position over the source solution, which was allowed to evaporate, under a hood, until just the source

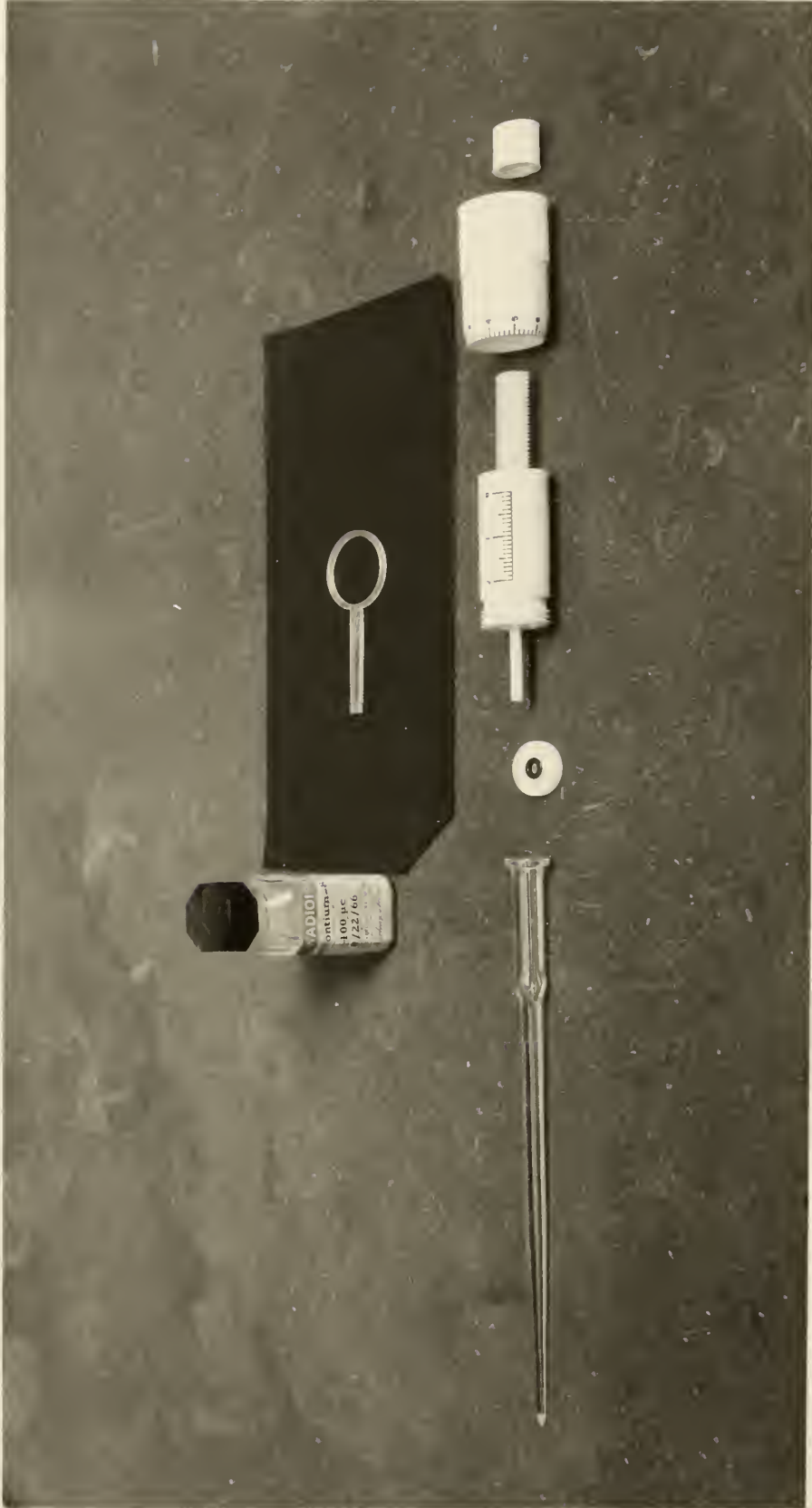


Figure 9. Source preparation apparatus.

residue was left on the mylar film. This process was repeated until the desired amount of material was dried onto the planchet.

The planchet was then removed to a counting cavity, which is described later, and counted. After counting, the entire process was repeated and the source was counted again. Then the remaining solution was dried onto the planchet, one drop at a time. It is important that this process be completed in one operation, so that the solution in the buret does not have an opportunity to evaporate. An  $\text{H}_2\text{SO}_4 + \text{KMnO}_4$  solution was used to clean the glass part of the buret immediately after the completion of a source preparation. This insured that the buret did not become radioactively contaminated in any measurable manner.

### 3.3 Procedure

The analyzer equipment and high voltage power supply were operated by 110 Volt, 60 Hz power. An intermatic switch automatically turned the equipment on at least two hours before the experiment day started. This allowed the equipment to warm up and the high voltage power supply to stabilize. Another intermatic switch turned on an air conditioner at about the same time so the room remained cool and the equipment did not become over heated. The pre-amplifier power supply was left on 24 hours a day since no intermatic switching was available.

At the beginning of the experiment day a series of standard tests were performed on the MCA (19) to determine if it was operating properly. In addition, a quality control run using a cobalt-60 and a cesium-barium-137 source was performed in order to determine the zero energy intercept. Such a run was performed about every two hours in order to maintain an accurate estimate of the zero energy intercept. The gain of the MCA was set so that

the photopeak of the calibration source under study was in the highest possible channel with the restrictions that the noise in the first few channels were maintained at a minimum and that no high energy counts were lost beyond channel 400.

The next step in the procedure was the positioning of the collimator and the source rack. This was one of the more critical steps in the experiment, since a relatively small error in the positioning could produce a large error in the accumulated spectra and hence in the final response function. The collimator was checked each morning to be sure that the barrel was level and that the collimator face was parallel to the source rack. The center position was checked and located with the aid of an optical level mounted on a tripod located about 15 feet behind the source rack. The source rack was also checked to be sure that it was level. This entire process was repeated at least twice daily. The positioning procedure allowed source placement to within  $1/8$  inch, the diameter of the largest source dot.

At least two spectra were accumulated at each source position for each calibration source used. A minimum live time was chosen so that at least 1,000 counts were registered in the maximum channel of the photopeak. This required runs of about 10 minutes at the center position, and runs as long as 1,000 minutes at the farthest radial position. Background runs were usually taken during the night for about 1,000 minutes. These runs were preceded and followed by quality control runs.

Five of the nine sources used, Pb-210, Hg-203, In-Sn-113, Cs-Ba-137, and Zn-65, emitted electrons. These electrons could be detected and contribute to the response which, of course, is undesirable. In order to eliminate these effects from the response, a  $1/4$ " thick lucite beta shield



was placed in front of the crystal face to absorb these electrons. However, the shield does have an effect on the gamma-ray flux incident on the shield. The total spectrum must be corrected for the flux attenuation. These corrections are discussed in detail in Appendix B.

## 4.0 RESULTS

### 4.1 Response Function Normalization

The response functions must be normalized in some consistent manner so they will be useful to other experimenters. In this study the responses are normalized to the unit uncollided flux per steradian at the source in a direction perpendicular to the source plane. The source strength of the plane is given as  $S_A$   $(\text{cm}^2\text{-sec})^{-1}$ . The uncollided flux is then given as

$$\phi^{\text{uc}} = \frac{S_A}{4\pi} (\text{cm}^2 \text{ sec sr})^{-1} \quad . \quad (4.1)$$

Before the point source responses were numerically integrated to give the infinite plane response functions, they were normalized to a unit point source strength, which had been previously determined by experiment. The integration process itself inherently normalizes the plane source responses to a unit area source strength. Therefore, in order to complete the normalization, the response functions are merely multiplied by  $4\pi$ . The units of the resulting response functions are counts/sec per  $(\text{cm}^2 \text{ sec sr})^{-1}$ . All of the response functions presented are on an energy scale of 3.5 keV per channel.

### 4.2 Two-Inch Collimator Results

Figure 10 shows the response function obtained for 1.114 MeV gamma rays. This result is considered typical of all nine two-inch response functions in that the data are smooth, which indicates good statistical results. Heath (7) shows a peak-to-valley ratio of approximately 28 for a point source response function of the same energy obtained in non-collimated geometry. Figure 10 shows a similar ratio of approximately 16. The difference is due to colli-

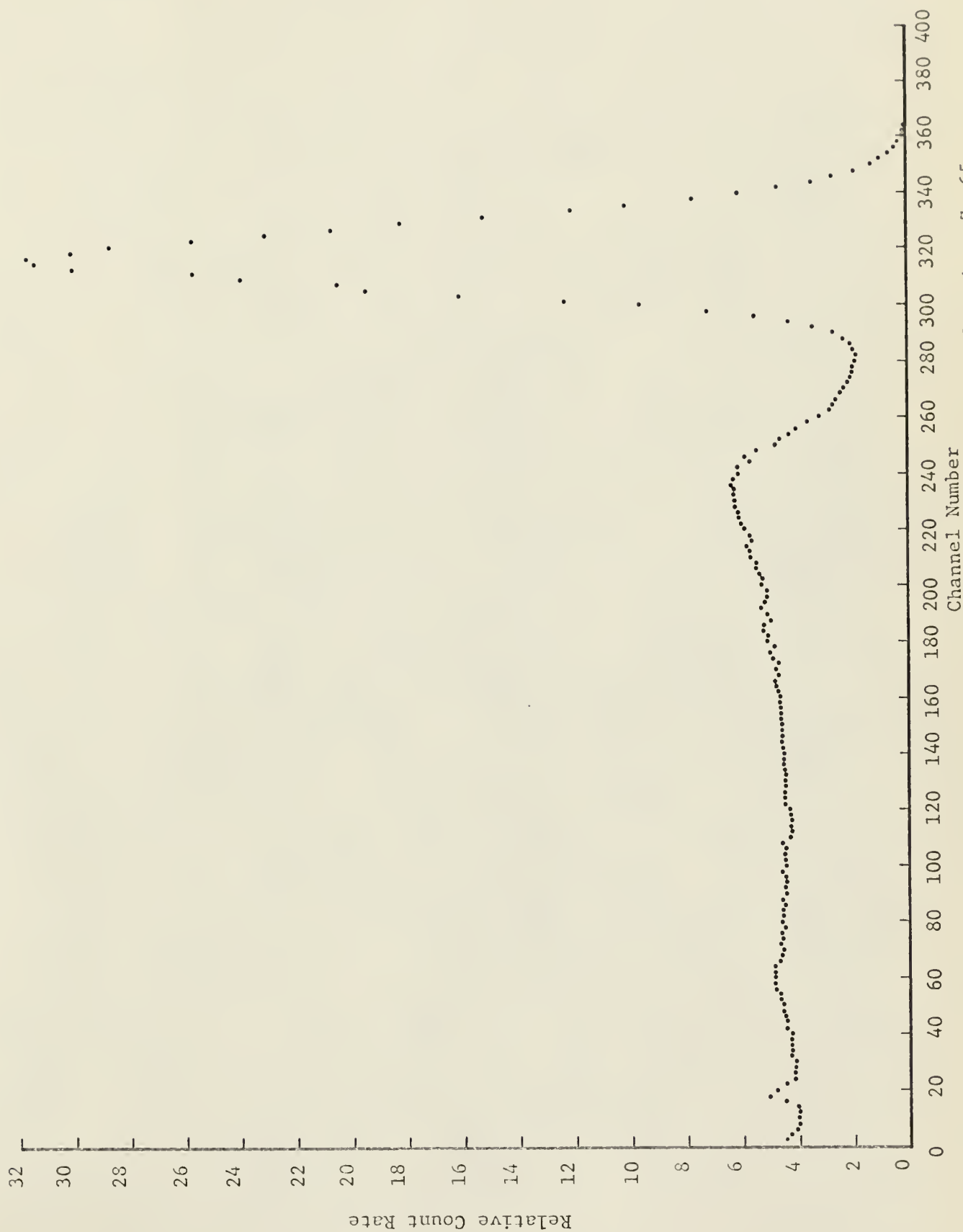


Figure 10. Typical two-inch collimator response function, Zn-65.

mator effects such as small angle scattering in the collimator barrel and the lucite beta shield. These effects tend to fill the valley between the photopeak and the Compton edge. The only error, however, is caused by scattering which occurs in the beta shield. The other effects introduced by the collimator are part of the system response. This error, however, is no larger than 1 percent in Figure 10.

The spectrum shape and other characteristics are in good agreement with those observed by Heath in his measurements, except for the following two facts. Zn-65 was used as the source, and this particular isotope emits a positron which is detected by the crystal. When the positron recombines with an electron in the crystal two 0.511 MeV photons are created. Since the positron is not very energetic, recombination takes place near the crystal face and one of the photons thereby created has a very good chance of escaping the detector. The other photon, however, has a very good chance of being detected; consequently a 0.511 MeV annihilation peak appears in the spectrum. This peak is not part of the system response and must therefore be removed from the spectrum. After the removal the response is no longer the response to a Zn-65 source, but rather the system response to a source of 1.114 MeV photons. The second characteristic to be noted is the small peak near channel 20. This peak occurs at approximately 70 keV on the energy scale and is caused by lead X rays. The 1.114 MeV photons interact with the collimator, which is constructed primarily of lead. The source photons are energetic enough to eject a K-shell electron from a lead atom and the subsequent internal conversion process of the atom causes the emission of a 72 keV X ray which is detected by the crystal. This peak is apparent in nearly all of the response functions and is a part of the system response. The peak does not appear at exactly

72 keV on the energy scale because of crystal non-linearities at and below this energy.

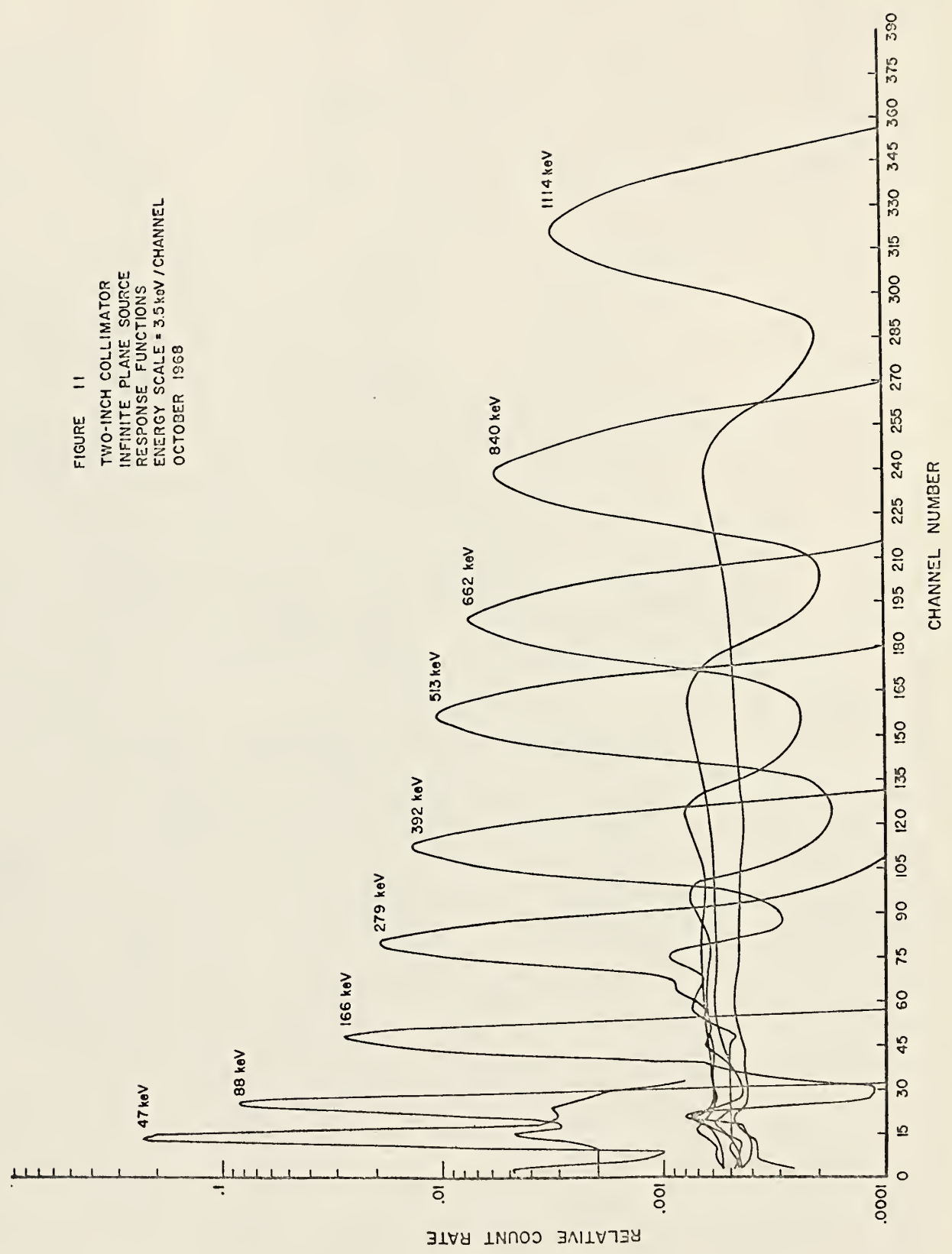
Figure 11 is a composite drawing of all nine two-inch collimator response functions. The general trends shown are relatively obvious. The photopeak amplitudes decrease with increasing energy, which is expected since the absorption cross section decreases with energy. This is shown more definitely in Figure 12. The lead X-ray peaks are apparent in most of the spectra around channel 15. These peaks are not obvious in the two lower energy response functions, either because they are not produced by the low energy source photons or because they are masked by poorly resolved iodine escape peaks.

Figure 12 shows the photopeak heights for the two-inch collimator as a function of energy. At lower energies photo absorption is the dominant photon interaction process in the crystal detector and increases very rapidly with decreasing energy. In the middle energy range Compton scattering becomes the dominant process and the absorption process decreases exponentially in NaI(Tl). Figure 12 is also a good indication of the consistency of the two-inch collimator data.

The width parameter of the photopeaks,  $B_0$ , is shown in Figure 13 as a function of energy. Above approximately 300 keV,  $B_0$  seems to be increasing in a linear manner, indicating that the system resolution is improving with energy. As energy decreases, the resolution decreases; i.e., the system cannot resolve peaks which are closely spaced. Inspection of Figure 13 indicates that  $B_0$  is tending toward zero at zero energy, which means that the  $W_0$  is zero at zero energy.

The actual response functions are tabulated in Appendix D with their appropriate variances. The standard deviations of the response functions

FIGURE 11  
TWO-INCH COLLIMATOR  
INFINITE PLANE SOURCE  
RESPONSE FUNCTIONS  
ENERGY SCALE = 3.5 keV / CHANNEL  
OCTOBER 1968





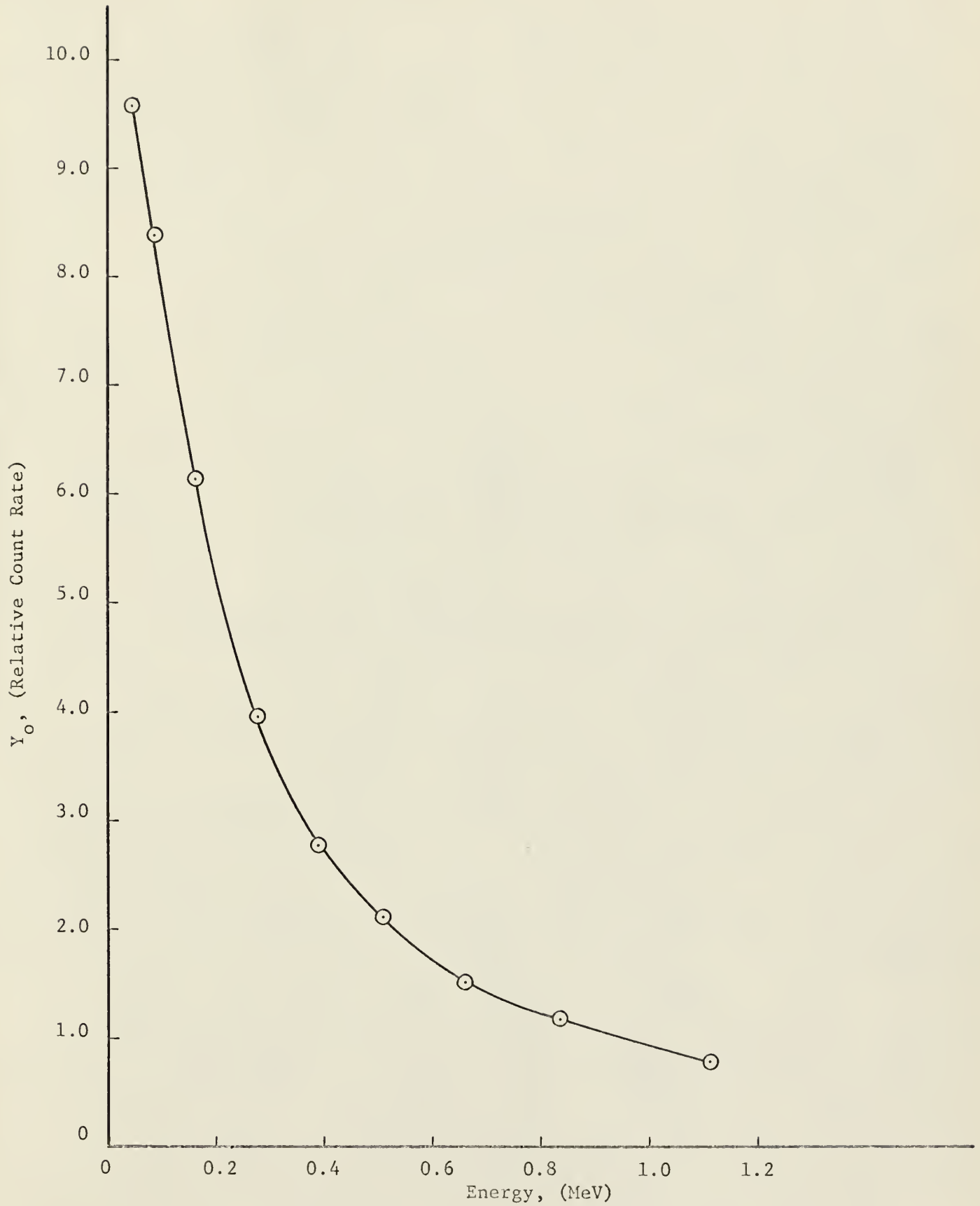


Figure 12. Photopeak amplitude as a function of energy, two-inch collimator.



Figure 13.  $B_0$  as a function of energy for two-inch collimator response functions.

for the two-inch collimator average somewhat below 5 percent. These standard deviations include the error in the source calibrations and the random error associated with the counting process. The standard deviations are indicative of the statistical processes of detection only and no estimate of the systematic error is included. These systematic errors could be caused by errors in the source positioning on the source rack, computer round-off error in the data analysis, and errors that may have occurred in measuring the source to detector distances. It is believed, however, that these types of errors are small in the two-inch collimator experiments and that the standard deviation would not be increased by more than one or two percent if these errors could be included.

#### 4.3 One-half Inch Collimator Results

The half-inch response functions were accumulated in the same manner as the two-inch responses and normalized in the same manner to the unit uncollided flux per steradian and are presented on the same energy scale as the two-inch responses, i.e., 3.5 keV/channel. There are only eight response functions however, instead of the nine obtained for the two-inch collimator experiments. The Hg-203 response function was not obtainable for the half-inch experiments because of MCA malfunctions which invalidated most of the data obtained.

If a point source is placed on the collimator center line, the observed countrate for the half-inch collimator should be approximately a factor of 16 lower than that observed with the two-inch collimator because the solid angle subtended is factor of 16 smaller.

It can be shown however, that the half-inch response to a plane source is approximately a factor of 256 less than the two-inch collimator

response to a plane source. Let  $R_1$  and  $R_2$  represent the two-inch and half-inch responses, respectively, for a plane source, and  $C_1$  and  $C_2$  represent the responses for a point source.

$$R_1 = 2\pi \int_0^{r_1} C_1(r) r dr$$

$$R_2 = 2\pi \int_0^{r_2} C_2(r) r dr \quad (4.2)$$

where  $r_1$  and  $r_2$  are the radii of the plane sources used for the two-inch and the half-inch collimators. For the purposes of illustration, it is assumed that the  $C_i$  are independent of  $r$ . In these experiments  $r_1$  was approximately four times  $r_2$ . We then have the following relationships,

$$R_1 \doteq \pi r_1^2 C_1$$

$$R_2 \doteq \pi r_2^2 C_2$$

$$r_1 \doteq 4r_2$$

$$C_1 \doteq 16C_2 \quad (4.3)$$

The ratios of the responses are computed as shown below;

$$\frac{R_1}{R_2} \doteq \frac{r_1^2 C_1}{r_2^2 C_2}$$

$$= \frac{(16r_2^2 \times 16C_2)}{r_2^2 C_2} = 256 \quad (4.4)$$

It was experimentally observed that the corresponding point source responses for the two collimators were related by approximately a factor of

sixteen.

Half-inch collimator experiments should also show improved system resolution because scattering in the collimator barrel should be reduced because of less surface area available for the scattering. Improved resolution was observed in this study as is shown in Figure 14. The half-inch resolution seems to be improved by approximately 13 percent over the two-inch experiments. It should be noted that the percent resolution of both collimators are smooth functions in the energy range of interest.

Figure 15 represents the photopeak amplitude as a function of energy for both collimators. The two inch results yield a smooth curve. As previously mentioned, the half-inch amplitudes should be approximately a factor of 256 below the two-inch amplitudes. With this in mind, such a curve was drawn on the same plot, based on the two-inch data, and then the half-inch data were plotted. The scattering of the half-inch data about the theoretical line is obvious, the worst case occurring at 166 keV, where the discrepancy is nearly a factor of two. It is believed that these discrepancies were caused by small errors in positioning the source on the source rack. A small error in positioning can make a large difference in the numerical integration of the point source data for the half-inch collimator. Figure 16 is a plot of the photopeak amplitudes for the point Ce-139 source as a function of the distance off center. It seems that the maximum of the distribution occurs somewhere between the assumed center and 1/4" off the center. The numerical integration was done from zero to 1.5 inches and gave an integrated amplitude of 0.000235, apparently much too high according to Figure 15. A second integration was done using 1/4" as the center location, this gave a value of 0.000147, a factor of 1.6 less than the previous calculation. This is a very large

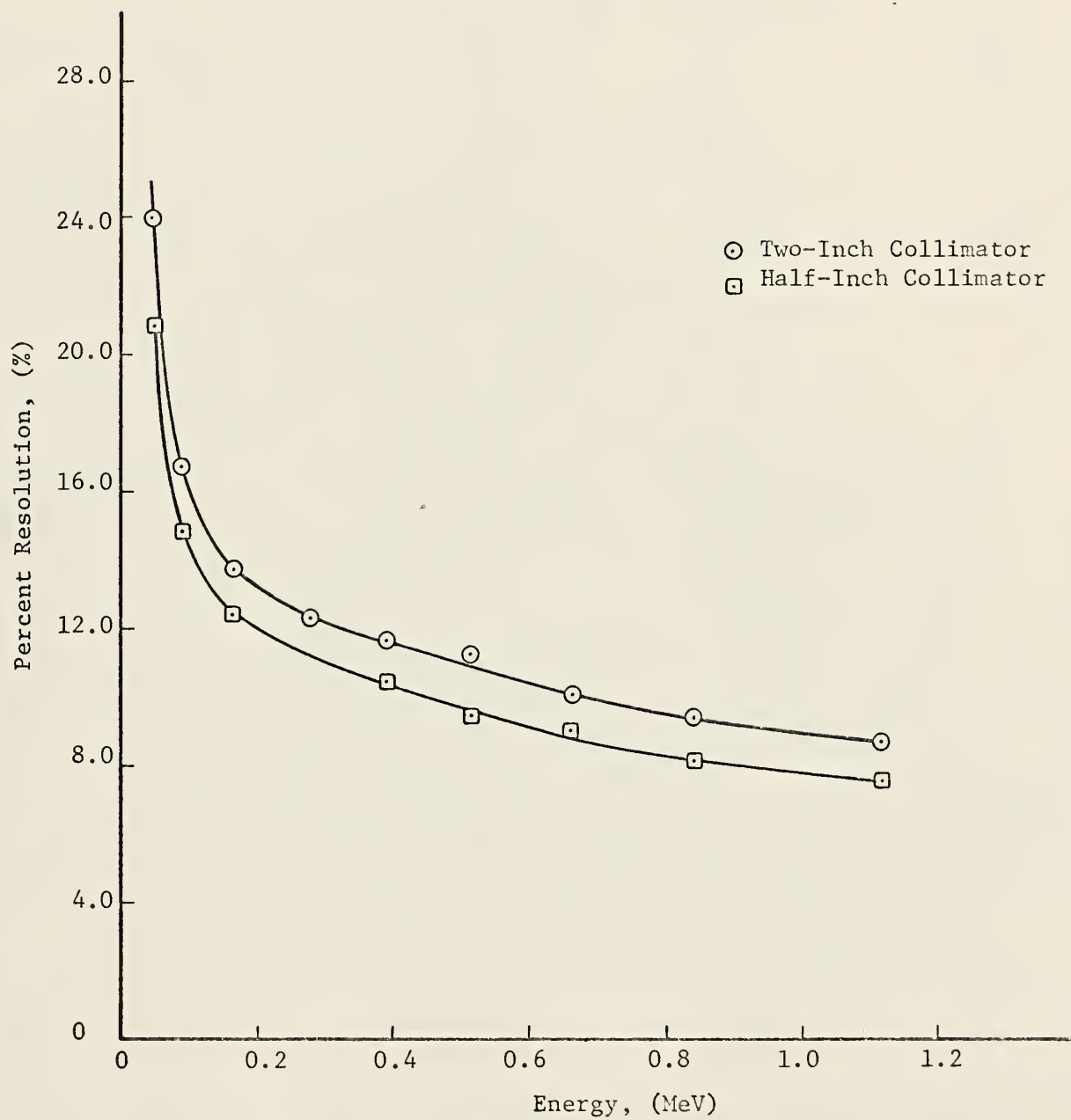
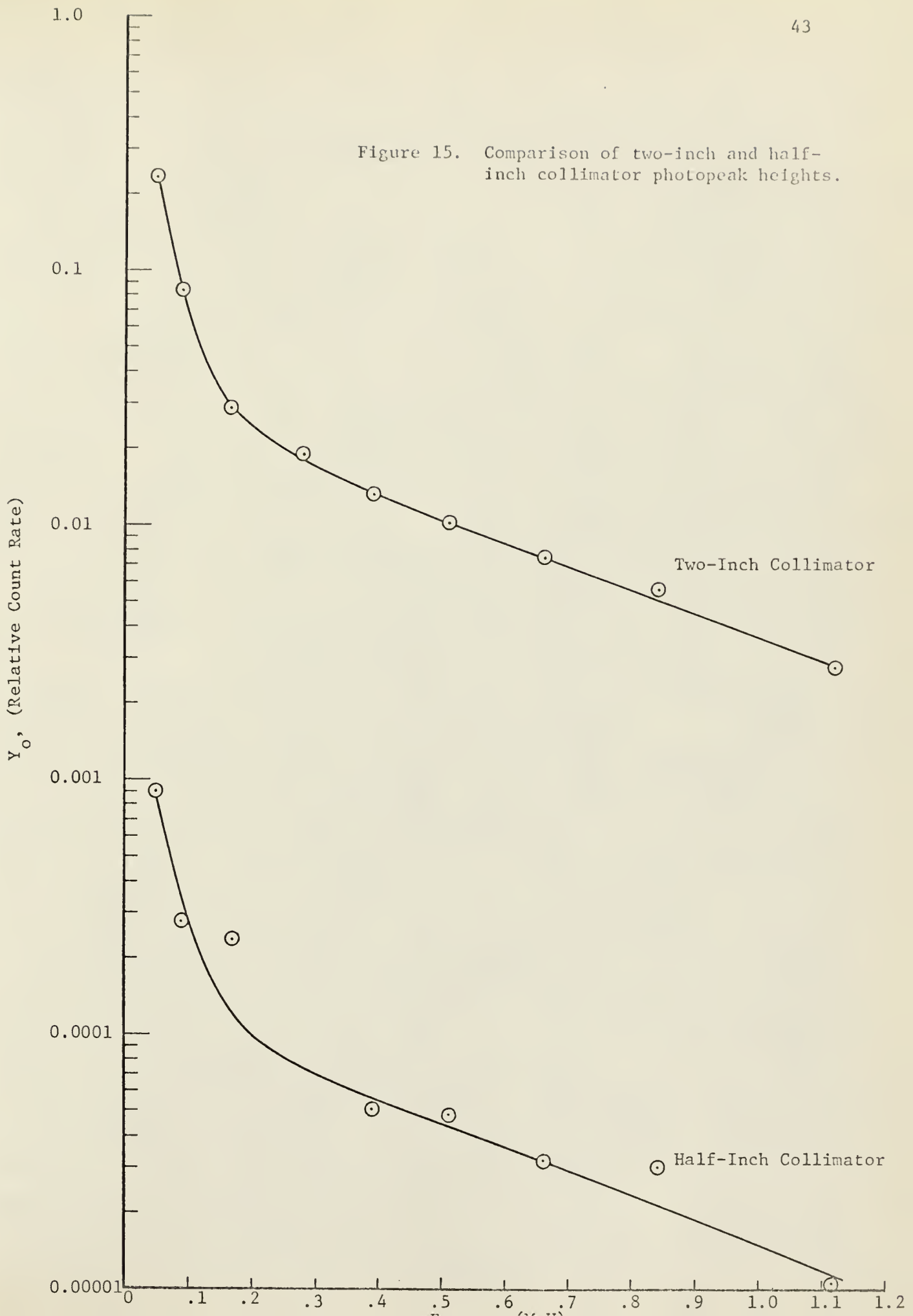


Figure 14. Percent resolution as a function of energy, two-inch and half-inch collimator response functions.



Figure 15. Comparison of two-inch and half-inch collimator photopeak heights.



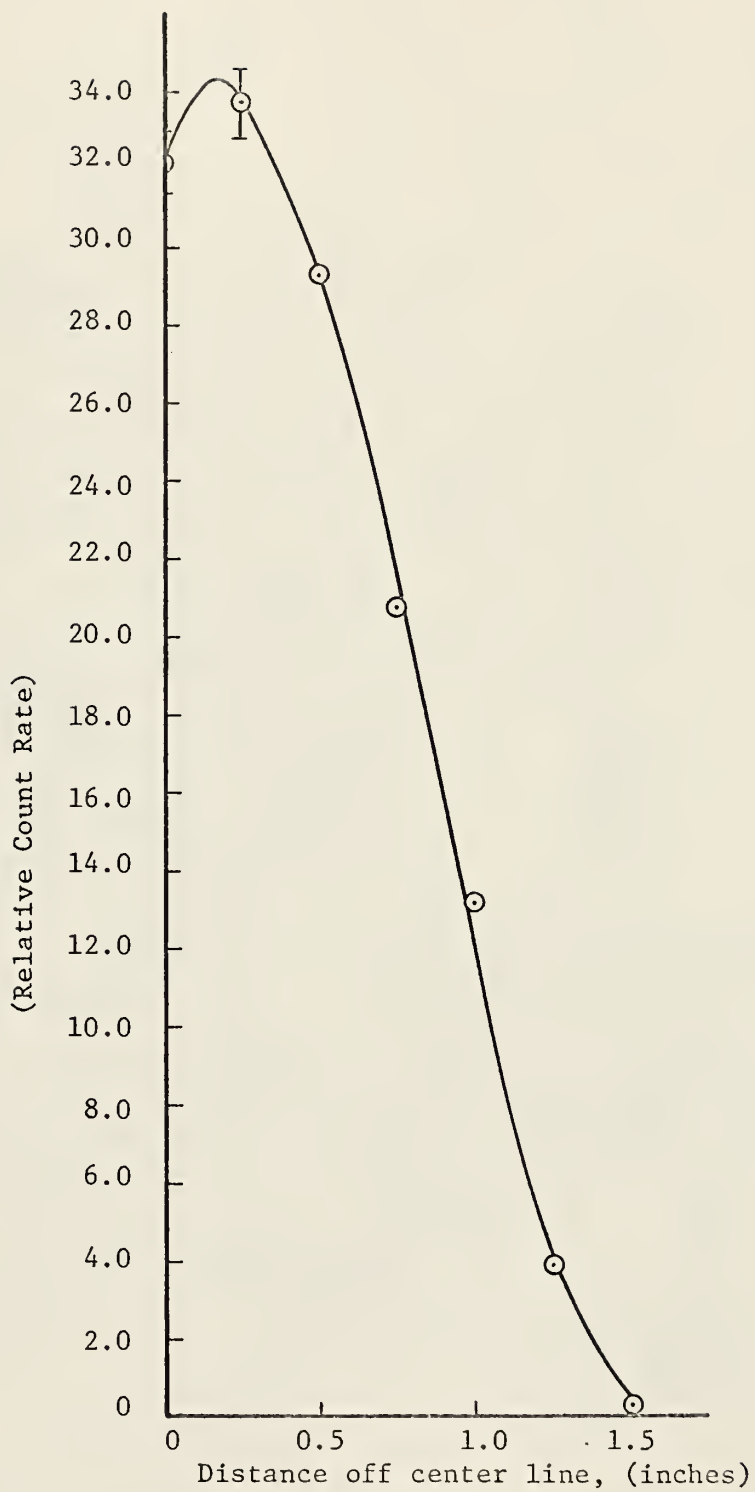


Figure 16. Photopeak response of half-inch collimator to Ce-139 Gamma Rays.

error for such a small error in positioning. Obviously positioning is very critical in the half-inch experiments. It seems as if these types of systematic errors are present in at least three of the half-inch experiments and hence the discrepancies noted. It should be noted that the source "dot" was approximately 0.125" in diameter for all the experiments, and an error of one or two source diameters near the center position will effect the final results drastically.

The half-inch collimator response functions obtained in this work are presented in tabular form in Appendix D together with their appropriate variances. The variances obtained in the half-inch experiments are not as good as those obtained with the two-inch collimator, and usually run around 10 percent. However, it is obvious that large systematic errors are present in some of the results, and in at least one case makes the statistical errors almost insignificant. The results are presented, however, as good "first" data for the half-inch collimator, since no attempt had been made previously at KSU to measure the half-inch response.

#### 4.4 Conclusions and Suggestions

The integrated point source method is capable of yielding consistent results which are both accurate and precise if extreme care is taken in the source positioning. This is supported by the fact that the two-inch collimator results obtained in this study agreed favorably with previously obtained data which were accumulated on the KSU system independently of this study using a completely different plane source simulation technique. The half-inch collimator results cannot be supported directly since no previous data are available. However, since the experimental technique was the same for both collimators, it is believed that good results are obtainable with the smaller collimator if a more accurate source positioning

technique is devised.

It was intended to accurately calibrate the two-inch collimator system in order to check previous experiments and provide accurate response functions for future experiments; this goal was achieved. It was also intended to obtain first data on the half-inch collimator system in order to observe general trends and relationships between the two systems. This goal was also achieved since some basic resolution and relative magnitude trends became apparent which were not obvious before the experiments were initiated.

A major disadvantage of the integrated point source method is the amount of data which must be accumulated in order to obtain reasonable results. In this study approximately 750 spectra were obtained over an eight month period. The data reduction and analysis required approximately ten hours of IBM 360/50 machine time and many more hours of manual data handling. It is believed that comparable results are obtainable using other, faster, means of plane source simulation, such as the plane simulator method described by Baran (1). The plane simulator method would probably be better for the half-inch experiments than the method used, since positioning should be somewhat easier, although not trivial by any means.

In this study, better statistical results could have been obtained if two different sets of sources had been used. The sources used were designed for the two-inch collimator experiments. These sources were not intense enough for the half-inch experiments because of the factor of sixteen reduction in the count rates. This resulted in long accumulation times for the half-inch experiments, which is usually undesirable. If the sources used had been sufficiently intense for the half-inch collimator, they would

have been too intense for the two-inch collimator experiments and would have caused large dead times in the counting system which could have invalidated the data because of rapid spectral shifts associated with large dead times.

Quality control during spectrometer experiments is a continuing requirement. The baseline and the energy per channel must be well known during the experiments or the accumulated data may be useless. In previous studies and in this study, so-called quality control experiments were performed using a combination Co-60-Cs-Ba-137 source for the calibrations. These experiments were done approximately every two hours during an experiment day. This process is very expensive both in time lost from actual experiments and in computer time required for the analysis of the quality control spectra. It is suggested for future work that a commercially available stabilizer be purchased for the collimator-spectrometer system. Such a feedback device could maintain the energy per channel and the zero intercept at preselected levels. This would greatly reduce the need for quality control experiments, but not eliminate the need. In this author's opinion, the savings in time and money would be significant.

The response functions presented in this work are valid only for the KSU spectrometer system as it presently stands. It is known that as the detector ages the resolution of the crystal becomes poorer (1). Eventually the response functions will not properly represent the system. Also, if the crystal detector is replaced for some reason the system will have changed significantly and the response functions presented will be invalid. It is suggested that a study be made as to whether or not existing response functions could be modified to reflect these system changes. The modifi-

cations of course would have to be based on experimental data. It is believed, however, that the effort required to accumulate the new data, on which to base the modifications, would be less than that required to accumulate a new set of response functions.



## 5.0 ACKNOWLEDGMENTS

The author wishes to express his deep appreciation for the guidance provided by Dr. R. E. Faw, under whose direction this study was accomplished. The financial support provided by the Department of Nuclear Engineering under their GRA program and the Office of Civil Defense through their fellowship program is greatly appreciated. The computing time provided by the Kansas State University Computing Center is also appreciated.

The assistance of Dr. N. D. Eckhoff and Mr. R. M. Rubin in the construction of the computer codes required for the analysis is also gratefully acknowledged. The efforts of Mr. R. E. Hightower in providing electronic support for the project were invaluable.

Finally, the assistance provided by Dr. W. R. Kimel, in arranging for the financial support required for the actual performance of the experiments, is highly appreciated.

6.0 LITERATURE CITED

1. Baran, J. A., "Reflection of Cobalt-60 Gamma Rays from Concrete", Ph.D. Thesis, Kansas State University, Department of Nuclear Engineering, (1968).
2. Beers, Y., "Introduction to the Theory of Error", Addison-Wesley, Reading, Mass., (June, 1962).
3. Birks, J. B., "The Theory and Practice of Scintillation Counting", Macmillian, New York, (1964).
4. Crouthamel, C. E., "Applied Gamma Ray Spectrometry", Macmillian, New York, (1960).
5. Eckhoff, N. D., "Optimal Neutron Activation Analysis", Ph.D. Thesis, Kansas State University, Department of Nuclear Engineering, (1968).
6. Gradshteyn, I. S. and I. M. Ryzhik, "Table of Integrals, Series, and Products", Academic Press, New York, (1965).
7. Heath, R. L., "Scintillation Spectrometry - Gamma-ray Spectrum Catalogue", second edition, IDO-16880, (August, 1964).
8. Heath, R. L. et al., "The Calculation of Gamma-ray Shapes for Sodium Iodide Scintillation Spectrometers -- Computer Programs and Experimental Problems", IDO-17017, (April, 1965).
9. Hubbel, J. H. and M. J. Berger, "Photon Attenuation and Energy Absorption Coefficients, Tabulations and Discussion", second edition, NBS report 8681, (Sept., 1966).
10. Kimel, W. R. (Editor), "Radiation Shielding, Analysis and Design Principles as Applied to Nuclear Defense Planning", OCD, TR-40, (Nov., 1966).
11. Mather, R. L., "Gamma-ray Collimator Penetration and Scattering Effects", J. Appl. Phys., 28, 1200 (1957).
12. O'Kelley, G. D. (Editor), "Applications of Computers to Nuclear and Radiochemistry", NAS-NS-3107, (1962).
13. Peelle, R. W. and T. A. Love, "Observation of Nonproportionality of Response for a NaI(Tl) Scintillation Crystal", ORNL-2801, (1959).
14. Price, W. J., "Nuclear Radiation Detection", second edition, McGraw-Hill, New York, (1964).
15. Scofield, N. E., "A Technique for Unfolding Gamma-ray Scintillation Spectrometer Pulse-height Distributions", USNRDL-TR-447, (June, 1967).

16. Shafroth, S. M. (Editor), "Scintillation Spectroscopy of Gamma Radiation", Gordon and Breach Science Publishers, New York, (1967).
17. Siegbahn, K., "Alpha, Beta, Gamma-ray Spectroscopy", North Holland Publishing Co., Amsterdam, (1965).
18. Storm, E. and H. I. Israel, "Photon Cross Sections from 0.001 to 100 MeV for Elements 1 through 100", LA-3753, (Nov., 1967).
19. Technical Measurements Corporation, "Instruction Manual, Models 402 and 404 - 400 Channel Pulse-Height Analyzers", Vol. 1, North Haven, Conn., (1962).
20. Vegors, S. H. et al., "Calculated Efficiencies of Cylindrical Radiation Detectors", IDO-16370, (Sept., 1958).
21. White, G. R., "X-ray Attenuation Coefficients from 10 keV to 100 MeV", NBS 583, (April, 1957).

## 7.0 APPENDICES

## 7.1 APPENDIX A

### Source Strength Calibration

Three methods were used to determine the source strengths of the nine isotopes used in this study. Four source strengths were determined from absolute counting experiments; two more were obtained by doing comparative counting experiments using National Bureau of Standards certified sources. The remaining three source strengths were based on a calibration line constructed using data from the other six sources.

Initially it was hoped that all of the sources could be calibrated using absolute counting. This was not possible since the sources were originally in liquid form; consequently if all of the liquid were dried on the planchet, five of the sources would have been too "hot" to count in the absolute counting geometry available. No reliable method for drying part of the source solution on the planchet and keeping an accurate account of the volumes used was available since the source volumes were typically less than 0.1 ml and buret surface tension and evaporation became critical in the volume measurements. Absolute counting was therefore only possible with the four sources, Hg-203, Sr-85, In-Sn-113, and Ce-139. Mn-54 and Cs-137 were calibrated by comparing the photopeaks of the experimental source spectra with those of the NBS certified source spectra, both pairs of which were accumulated under the same conditions. Cd-109, Pb-210, and Zn-65 were calibrated using a technique to be discussed later.

#### 7.1.1 Absolute Counting Theory

The detection efficiency,  $T(E)$ , of the crystal is the first major parameter of importance. For well defined source-detector geometries, this efficiency may be calculated from the known values of the absorption

cross sections,  $\tau(E)$  (20), for NaI. Equations have been derived for several cases (7,20). A monoenergetic point source of radiation located on the extended axis of a right circular cylindrical detector is of interest here. Figure 17 shows the configuration used in this experiment.

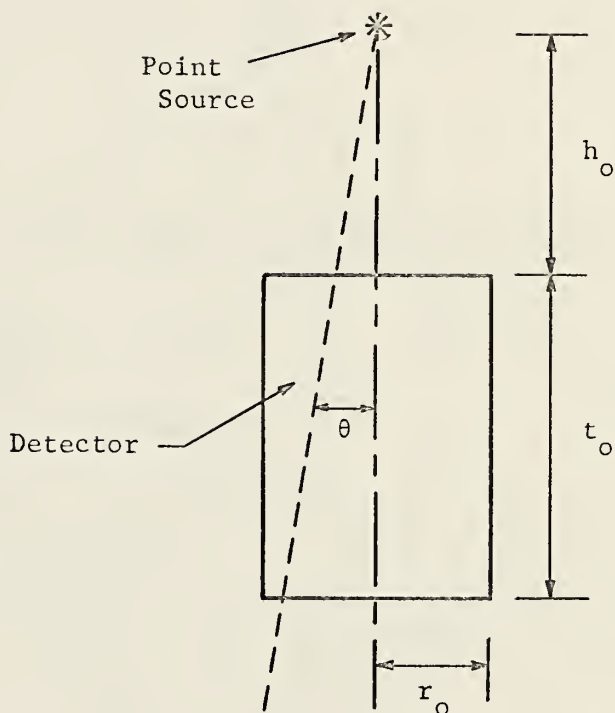


Figure 17. Source-detector geometry for absolute counting experiments.



Equation (A-1) is the analytical expression used to evaluate  $T(E)$ . The integral expressions were evaluated numerically using a 96 point Gaussian quadrature.

$$T(E) = 1/2 \left\{ \int_0^A \left[ 1 - \exp \left( - \frac{\tau(E)t_0}{\cos\theta} \right) \right] \sin\theta d\theta + \int_A^B \left[ 1 - \exp \left( -\tau(E) \left[ \frac{r_0}{\sin\theta} - \frac{h_0}{\cos\theta} \right] \right) \right] \sin\theta d\theta \right\} \quad (A-1)$$

where

$$A = \tan^{-1} \left( \frac{r_0}{h_0 + t_0} \right)$$

$$B = \tan^{-1} \left( \frac{r_0}{h_0} \right) .$$

The calculated absolute detection efficiency obtained from the above expression is the probability that a photon of energy  $E$  emitted from the source will interact in the detector with a finite energy loss. Any error to be expected will be due to the uncertainty in the tabulated values of  $\tau(E)$  used in the calculation. The maximum uncertainty in  $\tau(E)$  is at the higher energies, greater than 1 MeV, but it is still less than 10 percent, which results in an error of about 5 percent in  $T(E)$  (7,20). The error is reduced considerably at the lower energies, where a 3" x 3" crystal detector is practically opaque to gamma radiation of energies less than 200 keV.

The number of events observed in the pulse-height distribution is related to the emission rate of the source. The materials surrounding the detector may, however, scatter gamma rays into the crystal which tend to

mask this relationship. If such contributions do exist, they must be removed in order for this relationship to be clear. Since these contributions are of lower energy than the source energy, it is convenient to perform the calculations in terms of the photopeak efficiency,  $\epsilon_p(E)$ . This is defined as the probability that a gamma ray of energy E, emitted from the source will cause a count in the photopeak of the observed spectrum. The photopeak represents a more accurate measure of the emission rate because other contributions from scattering have virtually no effect on the photopeak in comparison to effects on the rest of the spectrum.

Direct calculation of  $\epsilon_p(E)$  represents a formidable problem because of the large number of multiple processes which can occur in the crystal. Consequently, it is convenient to use the following expression:

$$\epsilon_p(E) = T(E)P(E) \quad (A-2)$$

where  $T(E)$  is as before, and  $P(E)$  is defined as the fraction of the total number of events in the spectrum which appear in the photopeak, i.e., the peak-to-total ratio. The peak-to-total ratio is determined experimentally by careful measurement of monoenergetic sources under experimental conditions which reduce the scattering effects to an insignificant level.

The emission rate of a monoenergetic isotope is given by the following expression (7):

$$N_o = \frac{N_p}{T(E)P(E)A(E)t} \quad (A-3)$$

where  $N_o$  is the number of gamma rays emitted from the source per experiment.  $N_p$  is the total number of counts under the photopeak, and  $A(E)$  is an absorber correction factor used to account for the attenuation of the gamma rays caused by the insertion of a beta shield between the source and the detector,

and  $t$  is the experiment live time.

The absorber correction factor cannot be computed directly from tabulated cross section data, since these values are usually reported only for highly collimated geometries, it must therefore be measured experimentally for each source energy used. The best measure of  $A$ , as supported by the form of equation (A-3), is the ratio of the total number of counts in shielded and unshielded spectra.

### 7.1.2 Counting Procedure

The source-detector assembly was placed inside a large counting cavity with inside dimensions of 32" x 32" x 32". Figure 18 is a photograph of the partially completed cavity. The cavity is lead lined with cadmium and copper grading introduced to reduce the intensity of the characteristic lead X rays which may be produced in the lining. This type of shielding tends to minimize the scattering effects, which is desirable in any spectrum analysis.

The source was placed 10 cm above the crystal center by allowing the source planchet to rest on a plastic mount with a direct opening to the crystal face. Thus, a standard geometry (7) is achieved. The detector used was a Harshaw Integral Line assembly with a 3" x 3" NaI(Tl) scintillation crystal, operated at +900 volts. The output pulses from the photomultiplier tube are fed to a TMC 4096 multi-parameter system.

After initial planchet loading, the source was counted twice under the same conditions, except that one spectrum was accumulated with the beta shield. Figure 19 is a photograph of the detector assembly as placed in the counting cavity with the beta shield in place. The counting procedure was repeated several times in order to check the reproducibility of the counting experiment. After the source runs or during the source drying procedure

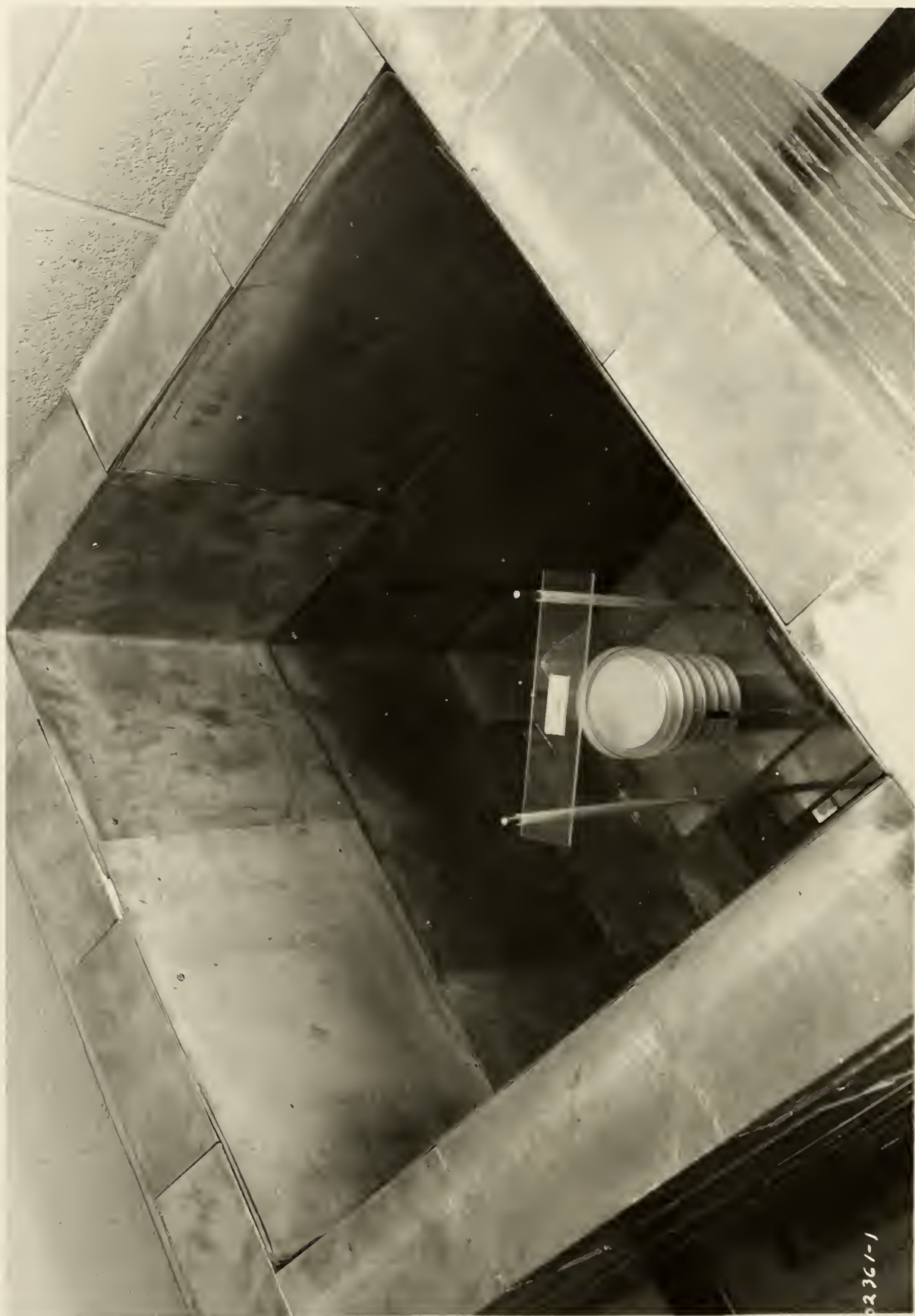


Figure 18. Counting cavity for absolute counting experiments.

02361-1



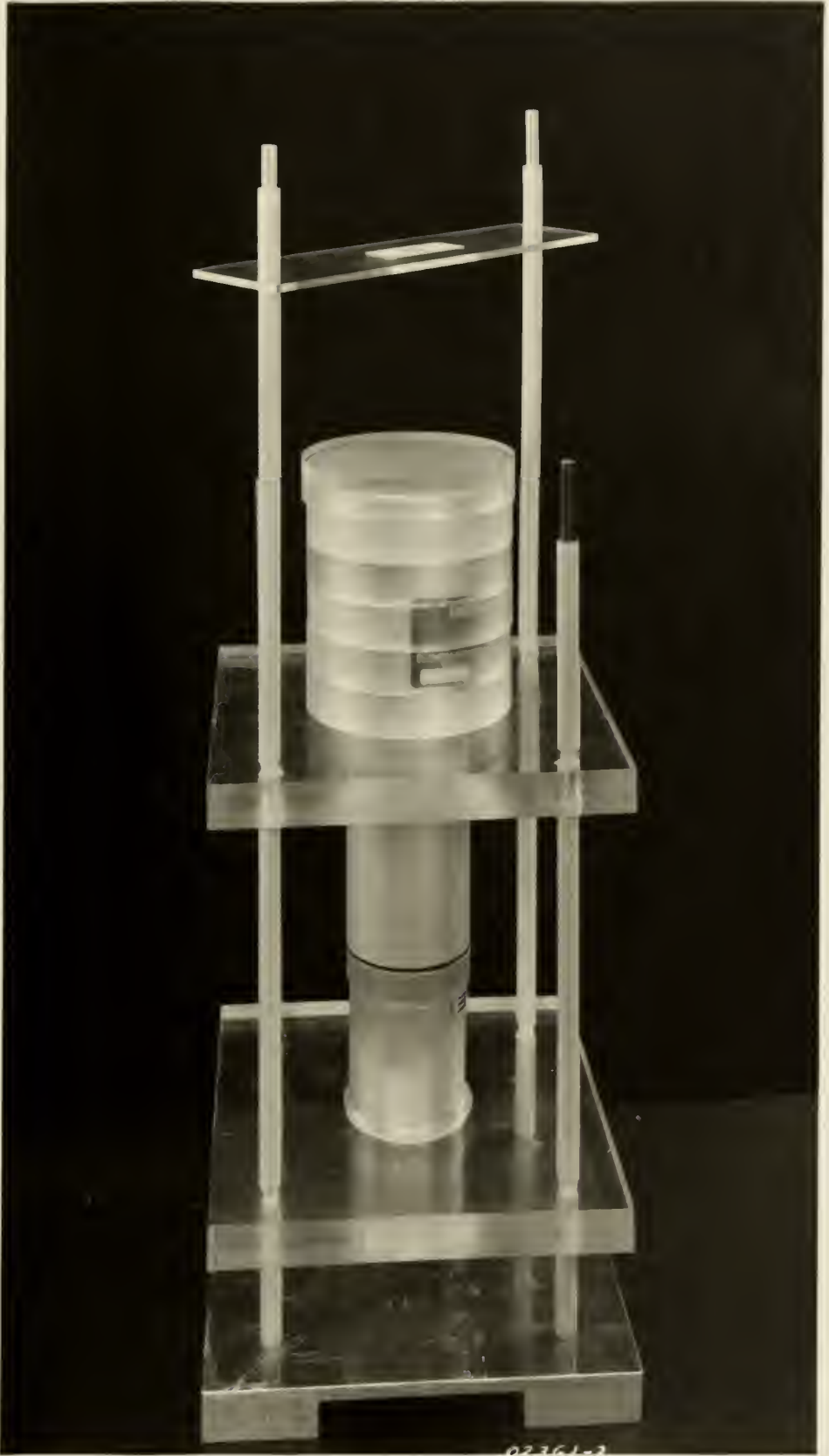


Figure 19. Detector assembly for absolute counting experiments.

background runs were made. These runs were relatively long (120 min.) so as to insure as small an error as possible in the background determination. Again, two runs were completed during each experiment day, one with the beta shield and one without the shield.

### 7.1.3 Data Analysis

Figure 20 shows a typical gamma-ray spectrum for Hg-203. This particular spectrum was obtained without the beta absorber in place and will be used to indicate how a typical analysis proceeded.

Backscatter and other wide angle scatter contributions are much reduced in the absolute counting geometry used, but are still visible and must be removed from the spectrum since they are not part of the response associated with the source energy. The broad peak in channel 70 of the Hg-203 spectrum is the backscatter peak. The characteristic 72 keV Tl X-ray peak in channel 40 and its associated iodine escape peak in channel 23 must also be removed since they also are not part of the crystal response to Hg-203 photons.

The Compton distribution on either side of the backscatter peak is very level and a straight line may be drawn between them. This procedure is illustrated in Figure 21. The procedure is a little more difficult in the region of the X-ray and the escape peak. A Compton distribution is still visible, but it is not constant from one side of the peaks to the other. Also, since the two peaks are not completely resolved, the distance between the extremes of the peaks is too great to warrant a simple averaging process. Consequently, since the Compton distribution is slightly increasing with decreasing energy, a least squares straight line was determined using four points on either side of the pair of peaks, the result being

$$Y(x_i) = -2.46x_i + 1100$$



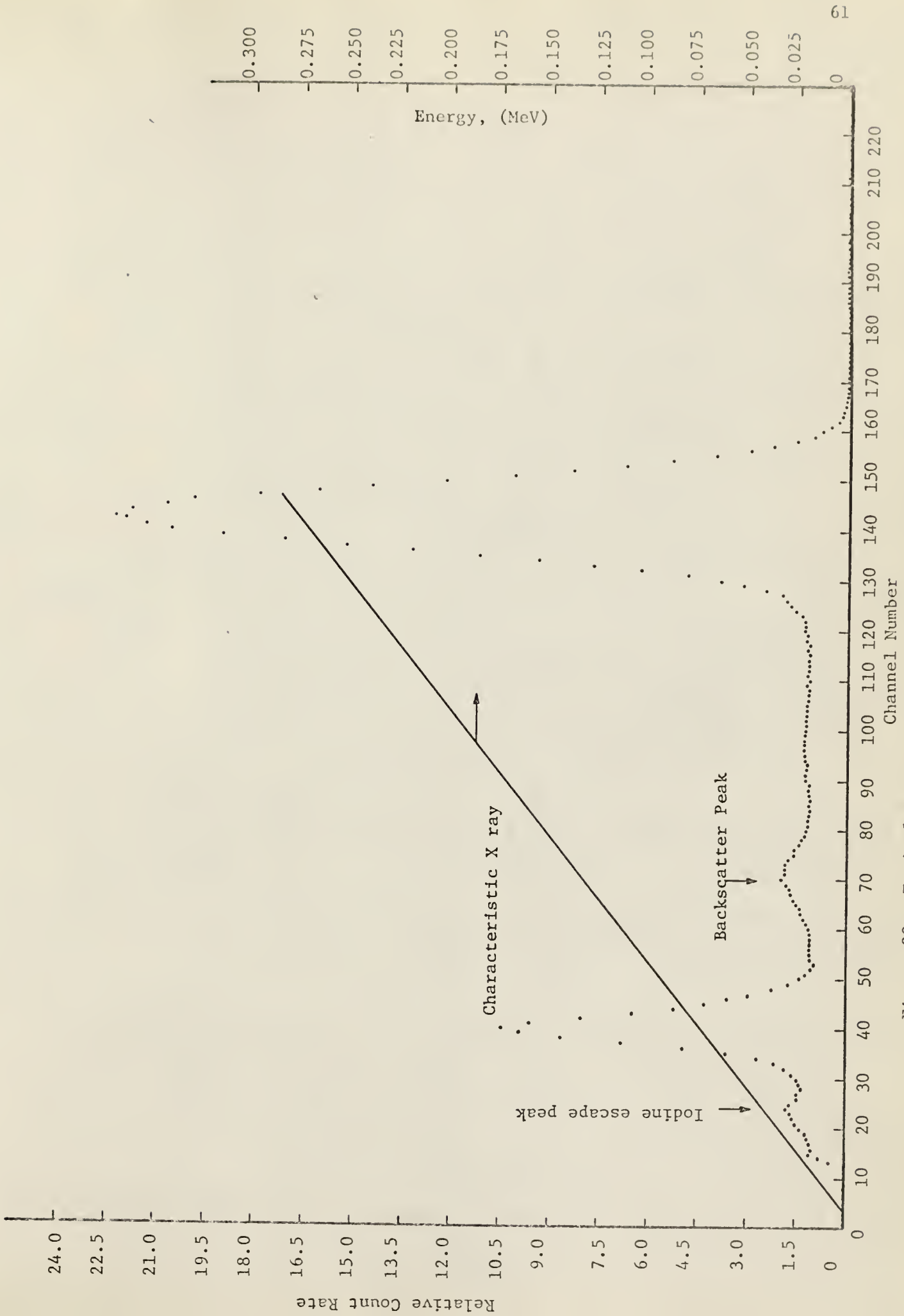


Figure 20. Typical spectrum obtained during absolute counting, Hg-203.



Figure 21. Illustration of spectrum correction technique, Hg-203 backscatter peak.

where  $i$  is the channel number and  $Y(x_i)$  is the calculated count rate in channel  $i$ .

Having subtracted the undesirable contributions from the "shielded" and "unshielded" spectra, one has a good representation of the corrected crystal response to 279 keV gamma rays for both shielded and unshielded experiments. The two types of spectra are corrected in the same manner. One is now equipped with the necessary experimental data to determine the absolute gamma-ray emission rate of the source.

The first step is to fit the photopeak to a Gaussian distribution and to determine the area under the photopeak. As stated in section 2.2, the fit is accomplished by the use of a polynomial least squares technique. The photopeak area is available from the fit parameters as

$$N_p = Y_o (\pi B_o)^{1/2} . \quad (A-5)$$

The total area is determined by integrating the entire spectrum, i.e., totaling the counts in the entire spectrum. The peak-to-total ratio is given simply as

$$P(E) = N_p / N_t \quad (A-6)$$

where  $N_t$  is the total area. The beta absorber correction factor is the only undetermined parameter. Inspection of the emission rate equation reveals the experimental quantities required to measure  $A$ .

$$A = (\text{total counts})_u / (\text{total counts})_s \quad (A-7)$$

where  $s$  refers to the "shielded" spectrum and  $u$  refers to the "unshielded" spectrum.

The standard deviations associated with each experimental quantity were calculated and the final emission rate is reported with a percent

standard deviation. It should be noted, however, that the standard deviations reported do not include the systematic errors associated with the experiments. Evidence is presented below which indicates that the systematic errors are smaller than the statistical errors.

In order to check the validity of the absolute counting technique described, three independent experiments were performed using NBS certified sources. The counting procedure for the NBS sources, Mn-54 and Cs-137, was the same as that for the experimental sources. The analysis of the data was done in the same manner in order to insure consistency. The NBS Cs-137 source was counted on two different days in order to check the reproducibility of the experiments. All of the results are normalized to the same count rate and corrected for radioactive decay. The results are shown below.

---

Table I

Verification of Absolute Counting Technique

Source Strengths, ( $\text{sec}^{-1}$ )

Isotope	NBS	Measured
Mn-54	$1.75 \times 10^4 \pm 1.0\%$	$1.81 \times 10^4 \pm 5.1\%$
Cs-137	$4.55 \times 10^4 \pm 1.5\%$	$4.48 \times 10^4 \pm 3.5\%$
Cs-137	$4.55 \times 10^4 \pm 1.5\%$	$4.40 \times 10^4 \pm 4.1\%$

---

These results are considered to be adequate proof of the validity of the technique used. The results also indicate that systematic errors in the absolute counting experiments were small.

#### 7.1.4 Comparative Counting Technique

Comparative counting is a relatively simple technique. Two NBS certified sources were available for use in this experiment, Mn-54 and Cs-Ba-137. The experiments were performed in collimated geometry. The source planchet was placed on the collimator face so that the source dot was in the center of the aperture. Several experiments were done with both the NBS sources and the corresponding experimental calibration sources under the same conditions. Each spectral photopeak was then fitted and the photopeak area calculated from the fit parameters. The photopeak areas were then averaged for each source and the appropriate standard deviations calculated. The emission rate for the calibration source was then calculated from the NBS source strength using the following expression.

$$\frac{N_o^{cal}}{N_p^{cal}} = \frac{N_o^{NBS}}{N_p^{cal}} \quad (A-8)$$

where  $N_o^{NBS}$  is the certified source strength for the given isotope and  $N_p^{NBS}$  is the calculated photopeak area for the NBS source,  $N_p^{cal}$  is the calculated photopeak area for the experimental calibration source, and  $N_o^{cal}$  is the required emission rate for the calibration source. The technique is valid because it can be shown that the photopeak area is directly proportional to the emission rate (7,20).

An expression for the standard deviation of the calculated source strength, derived from standard propagation of error techniques (2), is given on page 66:

$$\sigma_{N_o}^{cal} = \left[ \left( \frac{N_p^{cal}}{N_{NBS}^p} \right)^2 (\sigma_{N_o}^{NBS})^2 + \left( \frac{N_o^{NBS}}{N_{NBS}^p} \right)^2 (\sigma_{N_p}^{cal})^2 + \left( \frac{N_o^{NBS} N_p^{cal}}{(N_{NBS}^p)^2} \right)^2 (\sigma_{N_p}^{NBS})^2 \right]^{1/2} \quad (A-9)$$

After the calculation is complete, the calculated source strength for the calibration source is corrected for radioactive decay.

#### 7.1.5 Calibration Line Technique

$S_R(E)$  is considered to be a factor which accounts for collimator effects in the experimental spectra. These effects are primarily manifested in lip penetration and wall scattering in the collimator barrel.

It has been experimentally shown (1,11) that the following equation displays an approximately linear nature with energy.

$$S_R(E) = \frac{T(E)}{K(1-e^{-\mu(E)t}) [E_1(b(E)) - E_1(b(E)\sec\theta)]} \quad (A-10)$$

$T(E)$  is the total number of counts in the normalized spectrum due to an isotope emitting photons of energy  $E$ . The spectrum is normalized to a unit source strength and a unit live time. Mather (11) indicates that  $S_R(E)$  is unity at zero energy.  $K$  is a proportionality constant which assures this. The term  $(1-e^{-\mu(E)t})$  is representative of the crystal efficiency,  $\mu(E)$  is the total attenuation coefficient for gamma rays of energy  $E$ , and  $t$  is the crystal thickness (three inches).

The angle  $\theta$  is the maximum angle between the collimator center



line and a line drawn from the center of the crystal face to the outer edge of the collimator barrel.  $E_1(b(E))$  is the first order exponential integral for  $b(E)$  mean free paths in air from the source plane to the crystal face for the isotope emitting photons of energy  $E$ . The term  $[ E_1(b(E)) - E_1(b(E)\sec\theta) ]$  is proportional to the uncollided flux from a disk source at the crystal face.

The two previously discussed source calibration techniques provide enough information for the calculation of six points on the  $S_R(E)$  calibration line. These six points are then fitted with a straight line in the least squares sense, and normalized to unity at zero energy, the result being,

$$S_R(E) = 6.719 \times 10^{-4}E + 1.000$$

where  $E$  is in keV. The proportionality constant  $K$  is the device used to normalize the calibration line. Figure 22 shows the resultant calibration line.

With the calibration line at hand, the procedure used to calculate the remaining three source strengths is straight forward.  $S_R(E)$  is known for the three isotopes under consideration. Equation (A-10) may then be solved for  $T(E)$ , the total number of counts in the normalized spectrum, i.e., the ratio of the total count rate to the source strength. Since the count rate is known, the source strength may be determined directly.

The results of the three calibration techniques discussed are shown in Table II.

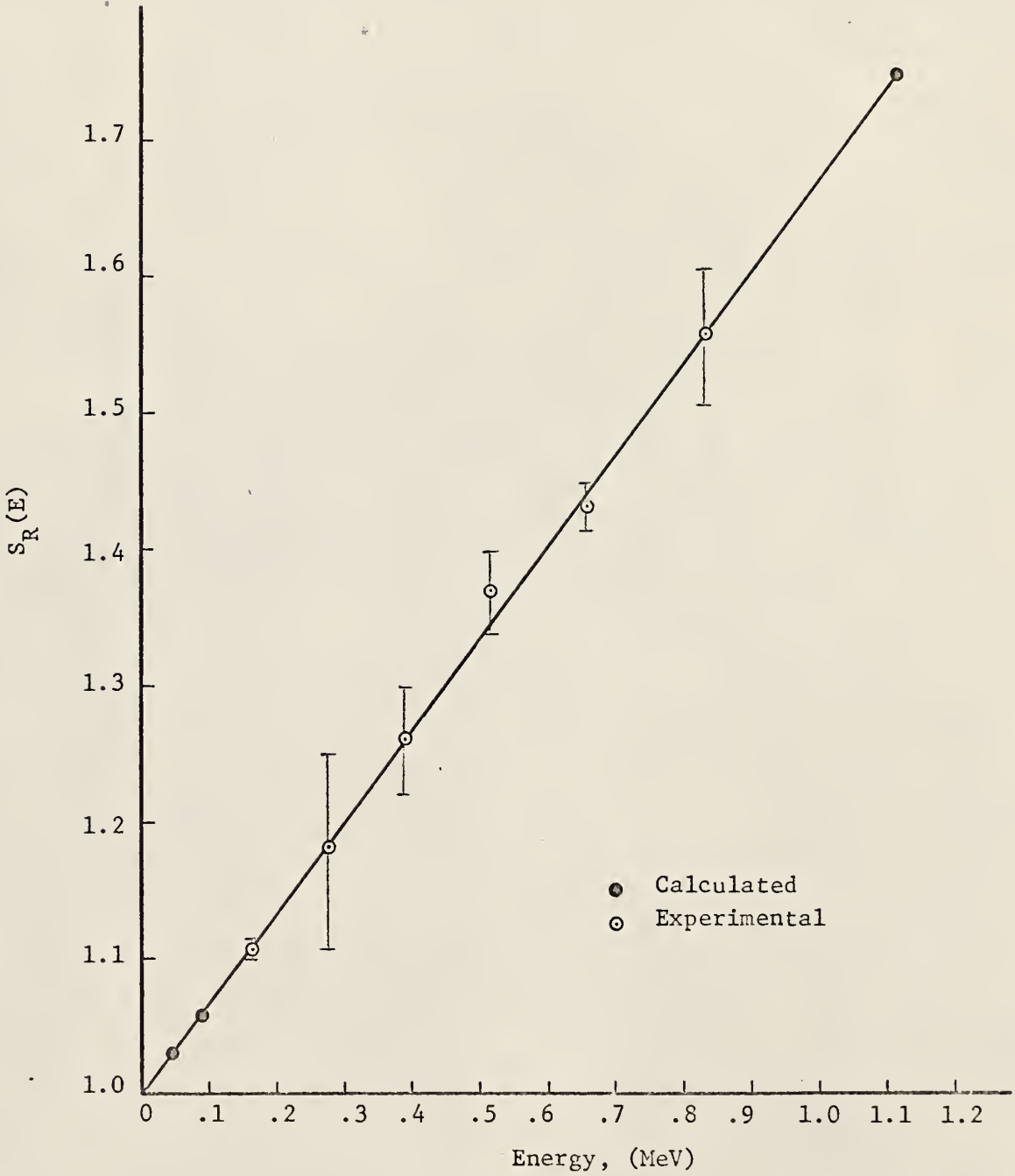


Figure 22. Lip penetration and wall scattering correction factor as a function of energy for the two-inch collimator response functions.

Table II

## Source Strengths of Experimental Isotopes

Isotope	E(keV)	Technique	Source Strength (min <sup>-1</sup> )
Pb-210	47	calib.*	$3.93 \times 10^6 \pm 5.6\%$
Cd-109	88	calib.	$2.85 \times 10^6 \pm 4.4\%$
Ce-139	166	abs.ct.**	$3.44 \times 10^7 \pm 1.1\%$
Hg-203	279	abs.ct.	$2.33 \times 10^7 \pm 5.8\%$
In-Sn-113	392	abs.ct.	$2.35 \times 10^7 \pm 3.0\%$
Sr-85	513	abs.ct.	$4.30 \times 10^6 \pm 2.5\%$
Cs-137	662	comp.ct.†	$1.42 \times 10^8 \pm 1.7\%$
Mn-54	840	comp.ct.	$8.16 \times 10^7 \pm 3.8\%$
Zn-65	1114	calib.	$1.32 \times 10^8 \pm 4.1\%$

\* Calibration line,  $S_R$

\*\* Absolute Counting

† Comparative Counting

## 7.2 APPENDIX B

### Beta Shield Correction Technique

The introduction of a beta shield into the spectrometer system produces two primary effects, (1) the entire gamma-ray energy spectrum is reduced by some constant factor, and (2) the valley between the photopeak and the Compton continuum tends to fill up because of small angle scatters in the beta shield. A third effect, the production of bremsstrahlung radiation in the shield, is possible but is considered to be a negligible effect.

Source energy photons which reach the beta shield may be lost from the system by absorption in the shield or by backscattering from the shield. It is necessary to derive an expression for the backscattering cross section; this is done by integrating the Klein-Nishina differential scattering cross section over the back hemisphere. The absorption cross section is then added to the backscattering cross section to obtain the total loss cross section. The derivation is outlined below.

$$\frac{d\sigma_c(\theta)}{d\Omega} = \frac{r_e^2}{2 [1+K(1-\cos\theta)]^2} \left\{ 1+\cos^2\theta + \frac{K^2(1-\cos\theta)^2}{1+K(1-\cos\theta)} \right\} \quad (B-1)$$

$$= \text{Klein-Nishina Compton scattering cross section, (cm}^2/\text{elec)/sr} \quad (18)$$

where  $K = E_0/m_0c^2$  and  $r_e$  is the classical electron radius. In order to simplify the integration process, the following change of variables is made.

$$\begin{aligned} u &= 1 - \cos\theta \\ du &= \sin\theta \, d\theta \end{aligned} \quad (B-2)$$

This leads to:

$$\frac{d\sigma_c(u)}{du} = \frac{r_e^2}{2} \left[ \frac{u^2 - 2u + 2}{(1+Ku)^2} + \frac{K^2 u^2}{(1+Ku)^3} \right] \quad (B-3)$$

$\sigma_{inc,BS}^{KN}$  = Klein-Nishina incoherent backscattering cross section

$$= \int_0^{2\pi} d\phi \int_{\pi/2}^{\pi} \frac{d\sigma_c(\theta)}{d\theta} \sin\theta d\theta$$

$$= 2\pi \int_1^2 \frac{d\sigma_c(u)}{du} du \quad (B-4)$$

$$= \pi r_e^2 \left\{ \int_1^2 \frac{u^2 du}{(1+Ku)^2} - 2 \int_1^2 \frac{udu}{(1+Ku)^2} + 2 \int_1^2 \frac{du}{(1+Ku)^2} + K^2 \int_1^2 \frac{u^2 du}{(1+Ku)^3} \right\} \cdot$$

The four integral expressions in equations (B-4) may be evaluated separately and then recombined to yield the final result. Equation (B-4) is rewritten as

$$\sigma_{inc,BS}^{KN} = \pi r_e^2 (I_1 - 2I_2 + 2I_3 + K^2 I_4) \quad (B-5)$$

where,

$$I_1 = \int_1^2 \frac{u^2 du}{(1+Ku)^2}$$

$$I_2 = \int_1^2 \frac{udu}{(1+Ku)^2}$$

$$I_3 = \int_1^2 \frac{du}{(1+Ku)^2}$$

$$I_4 = \int_1^2 \frac{u^2 du}{(1+Ku)^3} \quad (B-6)$$

With aid of tables of integrals (6), equations (B-6) are evaluated as

$$I_1 = \frac{1}{K^2} + \frac{1}{K^3} \ln \left[ \left( \frac{K+1}{2K+1} \right)^2 \right] + \frac{1}{K^2(K+1)(2K+1)}$$

$$I_2 = \frac{1}{2K^2} \ln \left[ \left( \frac{2K+1}{K+1} \right)^2 \right] - \frac{1}{K(K+1)(2K+1)}$$

$$I_3 = \frac{1}{(K+1)(2K+1)}$$

$$I_4 = \frac{1}{K^3} \left\{ \ln \left( \frac{2K+1}{K+1} \right) - \frac{2K}{(2K+1)(K+1)} + \frac{K(3K+2)}{2(2K+1)^2(K+1)^2} \right\} \quad (B-7)$$

Combining the four integrals according to equation (B-5), we write the expression for the backscattering cross section.

$$\sigma_{inc,BS}^{KN}(K) = \pi r_e^2 \left\{ \frac{1}{K^2} \left[ \frac{4K^2+5K+2}{(K+1)(2K+1)} - \frac{2(K+1)}{K} \ln \left( \frac{2K+1}{K+1} \right) \right] + \frac{\ln \left( \frac{2K+1}{K+1} \right)}{K} \right. \\ \left. - \frac{8K^2+9K+2}{2(2K+1)^2(K+1)^2} \right\} \text{ cm}^2/\text{elec} \quad (B-8)$$

The shield was made of lucite (polymethyl methacrylate,  $C_5H_8O_2$ ). For computational ease, the units should be converted from  $\text{cm}^2/\text{electron}$  to  $\text{cm}^2/\text{gm}$ , using the conversion factor  $f = 0.32501 \times 10^{24} \frac{\text{cm}^2/\text{g}}{\text{cm}^2/\text{elec}}$ , where



$$f = \frac{N_a Z}{A}$$

$$A = 100.06256 \text{ grams/g-mole}$$

$$Z = 54 \text{ electrons/molecule}$$

$$N_a = 0.60225 \times 10^{24} \text{ molecules/g-mole.}$$

For the five isotopes where the corrections are necessary, lucite displays an appreciable photoelectric absorption cross section only for the lead-210 energy. At this energy the cross section was evaluated as (18)

$$\sigma_{\tau,t}^{\text{Lucite}} (\text{Pb-210}) = 0.0185 \text{ cm}^2/\text{g} .$$

For mercury-203 the photoelectric cross section would increase the total loss cross section by less than 0.25 percent. Above the mercury-203 energy, no photoelectric cross sections are available for lucite(18). The total loss cross sections are as follows.

---

Table III

Total Beta Shield Loss Cross Sections

Isotope	Energy (MeV)	Cross Section ( $\text{cm}^2/\text{g}$ )
Pb-210	0.047	0.1023
Hg-203	0.279	0.0411
In-Sn-113	0.392	0.0337
Cs-137	0.662	0.0243
Zn-65	1.114	0.0170

---

The cross sections are converted to gamma-ray attenuation coefficients,  $\mu$  ( $\text{cm}^{-1}$ ), by multiplying them by the shield density which

was measured and found to be  $1.17 \text{ gm/cm}^3$ . Multiplying again by the shield thickness,  $1/4''$ , yields the number of mean free paths,  $\mu x$ . The whole spectrum is then multiplied by  $e^{\mu x}$  to account for the shield reduction effect.

The filling of the valley between the photopeak and the Compton tail is assumed to be a minor effect (see section 4.2). It is believed that a technique for correcting this filling effect could be developed, but such a development is beyond the scope of this work.

In order to check the accuracy of the multiplicative correction applied, data accumulated on the TMC 4096 multiparameter system were used. The data consisted of both "shielded" and "unshielded" spectra for the beta emitting isotopes. The table below compares the total area of the "unshielded" spectra to those of the corrected "shielded" spectra.

---

Table IV  
Comparison of Beta Shield Corrected Spectra

Isotope	Energy (MeV)	Cross section ( $\text{cm}^2/\text{g}$ )	$e^{\mu x}$	Percent Deviation*
Pb-210	0.047	0.1023	1.0997	-5.3
Hg-203	0.279	0.0411	1.0389	+2.0
In-Sn-113	0.392	0.0337	1.0318	-0.4
Cs-137	0.662	0.0243	1.0228	-0.2
Zn-65	1.114	0.0170	1.0159	+1.2

---

\* (corrected - unshielded) /unshielded

The correction seems to be very good in the middle energy range, poor in the lower energy range and adequate in the higher energy range. The

apparent loss of area in the lower energy range could be caused by the absorption of small angle scattered photons in the crystal containment can. It is also indicated (18) that the uncertainties in the scattering cross sections may be as high as 3 percent, and the uncertainties in the absorption cross sections may be as high as 10 percent. With these possible errors in mind, it is believed that the beta shield correction is adequate.

### 7.3 APPENDIX C

#### Spectrum Fitting Technique

The most important part of the gamma-ray spectrum is the photopeak. The photopeak amplitude is proportional to the source strength of the isotope, as is the photopeak area. The photopeak is less susceptible to spectral aberrations such as small angle scatters and bremsstrahlung; it is therefore the "cleanest" part of the spectrum. Consequently the photopeak is capable of yielding information about the gamma-ray emitting isotope under study.

As previously mentioned, the photopeak is approximately Gaussian in shape. The Gaussian shape has a physical basis in that the interactions in the crystal are statistical in nature and the detector and PM tube operate in a statistical manner. The photopeak is described then as,

$$Y(x_i) = Y_0 \exp\left[-\frac{(x_i - x_0)^2}{B_0}\right] \quad . \quad (C-1)$$

where  $Y(x_i)$  is the count rate in channel  $x_i$ .  $Y_0$  is the maximum photopeak amplitude, located at pulse height  $x_0$ .  $B_0$  is the photopeak width parameter equal to twice the variance of a normal Gaussian distribution. The fitting parameters to be solved for then, are  $Y_0$ ,  $x_0$  and  $B_0$ .

Equation (C-1) is non-linear and the least squares fit of the data may be accomplished in a non-linear manner by using an iterative process. This type of process is not very economical, however, if one has a large amount of data to be analyzed on a computer. An alternative is to linearize the problem by transforming the equation into the log domain, which results in a quadratic equation that may be fitted by using standard poly-

nomial least squares techniques. Comparisons between the two methods were made and the results were essentially the same, with the latter method requiring much less computer time than that required by the iterative method.

The basic input to the code used for the spectrum analysis is the spectrum itself, the number of channels of data (400), and the fitting limits. The fitting limits are very important, since these two parameters, the upper and lower limits, define between what channels the photopeak lies and therefore where the problem is to be solved.

It has been standard procedure (7) to base the limits on an estimate of the photopeak height. The lower limit is defined as that channel in which  $Y_0$  is reduced by approximately one third, the upper limit is that channel in which  $Y_0$  is reduced by approximately one half. The limits are chosen in this manner because small angle scatters and crystal nonlinearities cause the lower part of the photopeak to deviate from the Gaussian shape. The limits are not symmetric because small angle scatters affect only the lower energy side of the photopeak. This method of choosing the limits results typically in a fifteen channel fit of the photopeak using nine channels above  $x_0$  and six channels below.

### 7.3.1 Outline of Problem Formulation and Solution

Let L represent the lower fitting limit and U represent the upper limit. The least squares problem is represented in the log domain as

$$\overline{\mathbf{A}}\overline{\mathbf{S}} = \overline{\mathbf{B}}$$

where  $\overline{\mathbf{A}}$  is the coefficient matrix,  $\overline{\mathbf{S}}$  is the solution vector and  $\overline{\mathbf{B}}$  is the constants vector.  $\overline{\mathbf{A}}$  is a symmetric matrix and is formed as shown on page 78.

$$\begin{aligned}
A_{11} &= \sum_{i=L}^U (i-L)^4 W_i \\
A_{12} &= \sum_{i=L}^U (i-L)^3 W_i = A_{21} \\
A_{13} &= \sum_{i=L}^U (i-L)^2 W_i = A_{31} = A_{22} \\
A_{23} &= \sum_{i=L}^U (i-L) W_i = A_{32} \\
A_{33} &= \sum_{i=L}^U W_i \quad . \quad (C-3)
\end{aligned}$$

where  $W_i$  are the appropriate weighting factors, as previously discussed in section 2.2, in the log domain. The constants vector is set up in a similar manner, as shown below.

$$B_j = \sum_{i=L}^U (i-L)^{3-j} z_i W_i ; j = 1, 2, 3. \quad (C-4)$$

where  $z_i$  is the natural log of  $Y(x_i)$  and  $W_i$  is again the weighting factor.

The solution vector is obtained by premultiplying both sides of equation (C-2) by the inverse of the coefficient matrix,

$$\bar{S} = \bar{A}^{-1} \bar{B} \quad (C-5)$$

$$S_1 = -1/B_0$$

$$S_2 = 2x_0/B_0$$

$$S_3 = \ln Y_0 - (x_0/B_0)^2 \quad . \quad (C-6)$$



The fitting parameters are then given as

$$\begin{aligned} B_o &= -1/S_1, \\ x_o &= -1/2 \frac{S_2}{S_1}, \\ Y_o &= \exp \left( \frac{x_o^2}{B_o} + S_3 \right). \end{aligned} \quad (C-7)$$

The coefficient matrix is inverted by using a bordering method which is both fast and accurate for the 3 x 3 matrices under consideration.

If  $F_i$  represents the calculated photopeak height in channel  $i$ , the standard deviation of the fit is given as

$$\sigma = \left[ \frac{\sum_{i=L}^U (Y_i - F_i)^2}{(U-L+1)} \right]^{1/2}. \quad (C-8)$$

The extremes of each fit are checked in order to insure a good fit. If  $(Y_L - F_L)$  is greater than  $1.5\sigma$ ,  $L$  is replaced by  $L+1$  and the entire fit is redone. If  $(Y_U - F_U)$  is greater than  $1.0\sigma$ ,  $U$  is replaced by  $U-1$  and the problem solved again. This checking procedure was designed by Heath (7) and is considered to be an adequate criterion for obtaining a good fit.

The photopeak area is obtained by integrating the Gaussian equation from  $-\infty$  to  $+\infty$  as shown below.

$$N_p = \int_{-\infty}^{+\infty} Y(x) dx = Y_o (\pi B_o)^{1/2}. \quad (C-9)$$

The peak-to-total ratio is then immediately available as

$$p(E) = N_p / N_t. \quad (C-10)$$

The matrix formulation of the least squares problem provides a straightforward method for obtaining the variances of the fit parameters. The variances of  $S_i$  are taken from the diagonal elements of  $\bar{A}^{-1}$ , i.e.,  $A_{ii}^{-1}$  is the variance of  $S_i$ . The variances of the fit parameters are then immediately available by applying standard propagation of error techniques (2).

For more detailed information on the fitting techniques discussed, the reader is referred to Heath (7,8).

#### 7.4 APPENDIX D

##### Tabulated Response Functions

The response functions presented here are all normalized to a unit uncollided flux per steradian, such that the units are

$$(\text{counts/sec}) / (\text{cm}^2 \text{ sec sr})^{-1}$$

All the responses and their associated variances are tabulated on an energy scale of 3.5 keV/channel, with zero energy occurring at the beginning of channel two. Channel one is not part of the response function or its variance. The variances reflect all the mathematical operations performed on the response functions and are normalized in the same manner. Each listing is titled by the energy of the response, the collimator aperture used and whether or not the data are response functions or their associated variances.

Each page contains one complete response function or response function variance, i.e., 400 channels of data. Two hundred channels appear on the left half of the page under the title and are read from left to right. The remaining two hundred channels of data appear on the right half of the page, again, read from left to right.

























SV-113 RESPONSE FUNCTION VARIANCE, TWO-INCH COLLIMATOR	0.15975392E-11	0.164814482E-11	0.90843269E-12	0.69283235E-12
0.0	0.210549192E-10	0.10217007E-08	0.36230384E-09	0.72307794E-11
0.51613114E-03	0.29637241E-08	0.93346706E-07	0.18652918E-09	0.10229465E-11
0.57307248E-09	0.516326254E-09	0.33598302E-09	0.25885249E-09	0.97811603E-12
0.10975431E-09	0.16622683E-09	0.14838616E-09	0.23491151E-09	0.11350226E-11
0.14323398E-09	0.18023700E-09	0.219548134E-09	0.23909852E-09	0.0
0.22251976E-09	0.23113534E-09	0.20975303E-09	0.20099619E-09	0.0
0.19409449E-09	0.22479156E-09	0.24442515E-09	0.24622233E-09	0.0
0.22581829E-09	0.27023355E-09	0.19555806E-09	0.18463284E-09	0.0
0.18537324E-09	0.17108408E-09	0.15262899E-09	0.15664944E-09	0.0
0.15337597E-09	0.1339178E-09	0.13325015E-09	0.12147805E-09	0.0
0.11965912E-09	0.13126329E-09	0.13266312E-09	0.14929319E-09	0.0
0.19763926E-09	0.15685728E-09	0.15375996E-09	0.15157546E-09	0.0
0.15278179E-09	0.15462768E-09	0.14264178E-09	0.13885432E-09	0.0
0.13112942E-09	0.13610386E-09	0.14254403E-09	0.16872499E-09	0.0
0.13382094E-09	0.12149572E-09	0.23686719E-09	0.23843216E-09	0.0
0.21505517E-09	0.19035368E-09	0.17527862E-09	0.14791267E-09	0.0
0.11440703E-09	0.79470349E-10	0.73672999E-10	0.66577071E-10	0.0
0.60563359E-10	0.59554536E-10	0.52035806E-10	0.56274332E-10	0.0
0.59333410E-10	0.52302224E-10	0.49935039E-10	0.50562873E-10	0.0
0.5111723E-10	0.52198856E-10	0.52237520E-10	0.51925714E-10	0.0
0.52590657E-10	0.58817395E-10	0.72934894E-10	0.7547874E-10	0.0
0.7334391E-10	0.14014377E-09	0.19321066E-09	0.31195402E-09	0.0
0.56368865E-09	0.90508423E-09	0.16766202E-08	0.30021637E-08	0.0
0.66902677E-08	0.70356556E-08	0.10400541E-07	0.13652929E-07	0.0
0.17302483E-07	0.20054781E-07	0.22035010E-07	0.24068604E-07	0.0
0.21283796E-07	0.18944898E-07	0.16755571E-07	0.13219960E-07	0.0
0.10358129E-07	0.71608532E-08	0.49943942E-08	0.3182130E-08	0.0
0.13466824E-08	0.10167194E-08	0.62182082E-09	0.35681860E-09	0.0
0.2143394E-09	0.12669876E-09	0.66316314E-10	0.42548076E-10	0.0
0.26930805E-10	0.14290772E-10	0.1334992E-10	0.11089399E-10	0.0
0.67031370E-11	0.70444796E-11	0.56078623E-11	0.66919430E-11	0.0
0.47601584E-11	0.59391093E-11	0.50739664E-11	0.60704367E-11	0.0
0.57362727E-11	0.57708838E-11	0.51656708E-11	0.47071860E-11	0.0
0.69517916E-11	0.55985039E-11	0.54489226E-11	0.48416748E-11	0.0
0.35539213E-11	0.52592352E-11	0.3914654E-11	0.43037128E-11	0.0
0.27061227E-11	0.34886165E-11	0.27387285E-11	0.35864254E-11	0.0
0.29104979E-11	0.24126881E-11	0.27713369E-11	0.29343481E-11	0.0
0.26663111E-11	0.24126881E-11	0.2390082E-11	0.29669539E-11	0.0
0.39572894E-11	0.42058178E-11	0.37168419E-11	0.45217528E-11	0.0
0.41737945E-11	0.43933702E-11	0.50360903E-11	0.44993341E-11	0.0
0.63577477E-11	0.40225002E-11	0.54774518E-11	0.59339044E-11	0.0
0.54364597E-11	0.68794189E-11	0.55365374E-11	0.50299906E-11	0.0
0.53476258E-11	0.50334816E-11	0.53470258E-11	0.50861980E-11	0.0
0.50861980E-11	0.42597760E-11	0.58034836E-11	0.54122444E-11	0.0
0.28354991E-11	0.32277826E-11	0.358664254E-11	0.35945769E-11	0.0
0.24365366E-11	0.31625787E-11	0.14345695E-11	0.17260049E-11	0.0
0.16954016E-11	0.12715506E-11	0.23474793E-11	0.15649860E-11	0.0

SK-45	RESPONSE	FUNCTION, TWO-INCH COLLIMATOR	0.64163778E-05	0.3188117E-05	0.27933347E-05	0.22125425E-06
0.0	0.91256038E-03	0.72983140E-03	0.0	0.0	0.0	0.78821676E-06
0.83052134E-03	0.81045832E-03	0.77430718E-03	0.0	0.0	0.0	0.28763070E-05
0.77363150E-03	0.72201636E-03	0.81274449E-03	0.0	0.0	0.0	0.12583841E-05
0.43264926E-03	0.75102768E-03	0.97496037E-03	0.0	0.0	0.0	0.26530513E-05
0.87898030E-03	0.91887731E-03	0.91336662E-03	0.0	0.0	0.0	0.64163778E-05
0.83916627E-03	0.79121383E-03	0.82621745E-03	0.0	0.0	0.0	0.77439043E-05
0.62075366E-03	0.61352401E-03	0.78282575E-03	0.0	0.0	0.0	0.13717768E-04
0.77752955E-03	0.79816114E-03	0.77491420E-03	0.0	0.0	0.0	0.16372825E-04
0.62422364E-03	0.64668941E-03	0.87498093E-03	0.0	0.0	0.0	0.11726484E-04
0.83052745E-03	0.64638034E-03	0.81539061E-03	0.0	0.0	0.0	0.40240639E-05
0.81915636E-03	0.83391066E-03	0.86918403E-03	0.0	0.0	0.0	0.0
0.88546006E-03	0.85178909E-03	0.88660815E-03	0.0	0.0	0.0	0.0
0.88425074E-03	0.87398244E-03	0.87341573E-03	0.0	0.0	0.0	0.0
0.84473027E-03	0.91344440E-03	0.81113746E-02	0.0	0.0	0.0	0.0
0.83442697E-03	0.85404166E-03	0.83103077E-03	0.0	0.0	0.0	0.0
0.85099703E-03	0.87837791E-03	0.84673963E-03	0.0	0.0	0.0	0.0
0.81864116E-03	0.83896867E-03	0.82375715E-03	0.0	0.0	0.0	0.0
0.82586589E-03	0.86975093E-03	0.82793366E-03	0.0	0.0	0.0	0.0
0.86363667E-03	0.91311708E-03	0.90802740E-03	0.0	0.0	0.0	0.0
0.92108198E-03	0.76340990E-03	0.96652238E-03	0.0	0.0	0.0	0.0
0.10233019E-02	0.10125008E-02	0.10294163E-02	0.0	0.0	0.0	0.0
0.98198117E-03	0.10164513E-02	0.95028686E-03	0.0	0.0	0.0	0.0
0.87572429E-03	0.83525344E-03	0.75270678E-03	0.0	0.0	0.0	0.0
0.65424852E-03	0.59366871E-03	0.53521432E-03	0.0	0.0	0.0	0.0
0.47569675E-03	0.37745922E-03	0.38534193E-03	0.0	0.0	0.0	0.0
0.33763400E-04	0.32612391E-03	0.29957853E-03	0.0	0.0	0.0	0.0
0.26439893E-03	0.26999833E-03	0.25221612E-03	0.0	0.0	0.0	0.0
0.25245128E-03	0.24625599E-03	0.24227357E-03	0.0	0.0	0.0	0.0
0.22727823E-03	0.24537090E-03	0.22324572E-03	0.0	0.0	0.0	0.0
0.24473504E-03	0.22986337E-03	0.26152260E-03	0.0	0.0	0.0	0.0
0.24476764E-03	0.25643385E-03	0.26639039E-03	0.0	0.0	0.0	0.0
0.28332777E-03	0.34945714E-03	0.37711013E-03	0.0	0.0	0.0	0.0
0.58607386E-03	0.80779740E-03	0.10447621E-02	0.0	0.0	0.0	0.0
0.14668712E-02	0.24439483E-02	0.31570781E-02	0.0	0.0	0.0	0.0
0.47956893E-02	0.56570321E-02	0.67940541E-02	0.0	0.0	0.0	0.0
0.10211099E-01	0.10895644E-01	0.11799935E-01	0.0	0.0	0.0	0.0
0.13277035E-01	0.13678826E-01	0.13519518E-01	0.0	0.0	0.0	0.0
0.13617927E-01	0.12042437E-01	0.10935925E-01	0.0	0.0	0.0	0.0
0.90908967E-02	0.76465495E-02	0.65031089E-02	0.0	0.0	0.0	0.0
0.44649132E-02	0.36263615E-02	0.29433467E-02	0.0	0.0	0.0	0.0
0.17939298E-02	0.14401097E-02	0.10841459E-02	0.0	0.0	0.0	0.0
0.60159061E-03	0.47459034E-03	0.34493534E-03	0.0	0.0	0.0	0.0
0.17036583E-03	0.11615852E-03	0.76332741E-04	0.0	0.0	0.0	0.0
0.53986019E-04	0.26329246E-04	0.27103641E-04	0.0	0.0	0.0	0.0
0.24337967E-05	0.11062715E-05	0.92926821E-05	0.0	0.0	0.0	0.0
0.12411500E-04	0.84076653E-05	0.0	0.0	0.0	0.0	0.0
0.62089484E-05	0.90990370E-05	0.10177702E-04	0.0	0.0	0.0	0.0
0.52133024E-05	0.99564514E-05	0.0	0.0	0.0	0.0	0.0
0.21019157E-05	0.44623480E-05	0.95139412E-05	0.0	0.0	0.0	0.0
0.22125425E-06	0.20742573E-06	0.14260519E-06	0.0	0.0	0.0	0.0













HW-54 RESPONSE FUNCTION VARIANCE, TWO-INCH GULLIMATOR

0.0	0.3778173E-09	0.34885006E-09	0.31379432E-09	0.46496031E-10	0.43507545E-10	0.41920203E-10	0.41462733E-10
0.2	0.248411420E-09	0.21842817E-09	0.19192585E-09	0.42033849E-10	0.41536719E-10	0.42101322E-10	0.45624005E-10
0.4	0.21126059E-09	0.221068776E-09	0.22112636E-09	0.534662650E-10	0.44203540E-10	0.46373252E-10	0.49505289E-10
0.6	0.24139202E-09	0.23810415E-09	0.22132363E-09	0.100465234E-09	0.54731020E-10	0.624441716E-10	0.76650711E-10
0.8	0.42103451E-09	0.32010722E-09	0.31041939E-09	0.33262808E-09	0.46180415E-09	0.66180372E-09	0.921794737E-09
1.0	0.29452751E-09	0.28622216E-09	0.2590324E-09	0.12708805E-09	0.17895604E-09	0.24208560E-09	0.29447499E-09
1.2	0.23889804E-09	0.22655645E-09	0.21340693E-09	0.45453791E-09	0.47426196E-09	0.54971458E-09	0.66843917E-09
1.4	0.22740244E-09	0.22307803E-09	0.2190684E-09	0.74034716E-09	0.82761815E-09	0.90144371E-09	0.92361621E-09
1.6	0.22901592E-09	0.227991438E-09	0.23247347E-09	0.10035233E-09	0.10277760E-09	0.10274307E-09	0.99816047E-09
1.8	0.2319675E-09	0.23322251E-09	0.23094361E-09	0.96744256E-09	0.70152596E-09	0.846527640E-09	0.75071049E-09
2.0	0.2350961E-09	0.23717162E-09	0.24522162E-09	0.67440315E-09	0.56625948E-09	0.49735220E-09	0.40549097E-09
2.2	0.2390166E-09	0.24004421E-09	0.2390070E-09	0.35062886E-09	0.27935736E-09	0.21526800E-09	0.15426924E-09
2.4	0.24571678E-09	0.24672497E-09	0.25109670E-09	0.12672434E-09	0.43299080E-09	0.76180194E-09	0.54362444E-09
2.6	0.26012429E-09	0.26670812E-09	0.26616065E-09	0.41793409E-09	0.31817460E-09	0.22181319E-09	0.16391676E-09
2.8	0.26337914E-09	0.25791290E-09	0.26798083E-09	0.12664488E-09	0.4848679E-09	0.63464434E-09	0.64378955E-09
3.0	0.25106695E-09	0.24785621E-09	0.24065806E-09	0.41913112E-09	0.30737261E-09	0.26931207E-09	0.20706608E-09
3.2	0.23196965E-09	0.22842604E-09	0.23210062E-09	0.17329152E-09	0.20169991E-09	0.14374660E-09	0.16760981E-09
3.4	0.22530036E-09	0.21912167E-09	0.22937198E-09	0.12840621E-09	0.11619512E-09	0.12056584E-09	0.10834274E-09
3.6	0.20846139E-09	0.20834770E-09	0.21074834E-09	0.11363395E-09	0.45488019E-09	0.97725118E-09	0.10681542E-09
3.8	0.2319555E-09	0.24738073E-09	0.24605273E-09	0.91475230E-09	0.88634499E-09	0.95452457E-09	0.99429664E-09
4.0	0.24275860E-09	0.24156421E-09	0.23684169E-09	0.10319475E-09	0.11313672E-09	0.97227998E-09	0.96979466E-09
4.2	0.22509545E-09	0.22118857E-09	0.19783647E-09	0.10113414E-09	0.97725118E-09	0.87498025E-09	0.87498025E-09
4.4	0.20999545E-09	0.19891662E-09	0.26437638E-09	0.10056600E-09	0.99997788E-09	0.10170226E-09	0.91475230E-09
4.6	0.21391593E-09	0.19954094E-09	0.19946771E-09	0.97725118E-09	0.72725636E-09	0.80111915E-09	0.82917154E-09
4.8	0.20306459E-09	0.19130256E-09	0.19590113E-09	0.75566519E-09	0.98861431E-09	0.86113193E-09	0.85793551E-09
5.0	0.2007767E-09	0.19829099E-09	0.1947613E-09	0.62917154E-09	0.94493666E-09	0.81993691E-09	0.96020546E-09
5.2	0.19325335E-09	0.20713121E-09	0.20823396E-09	0.83343367E-09	0.79685772E-09	0.90907091E-09	0.73151735E-09
5.4	0.20679679E-09	0.21550654E-09	0.20816646E-09	0.84556417E-09	0.65900098E-09	0.85225412E-09	0.67498025E-09
5.6	0.20124553E-09	0.21982463E-09	0.20351809E-09	0.73293776E-09	0.78407450E-09	0.90111915E-09	0.80360415E-09
5.8	0.20291454E-09	0.20891590E-09	0.20260707E-09	0.75566515E-09	0.80111915E-09	0.82388454E-09	0.86928664E-09
6.0	0.20431354E-09	0.21062037E-09	0.20817006E-09	0.10227036E-09	0.465518876E-12	0.43542270E-12	0.38796511E-12
6.2	0.20595033E-09	0.19851935E-09	0.21079079E-09	0.0	0.0	0.0	0.0
6.4	0.21491708E-09	0.20221140E-09	0.22471108E-09	0.0	0.0	0.0	0.0
6.6	0.21527928E-09	0.22124512E-09	0.23044937E-09	0.0	0.0	0.0	0.0
6.8	0.23556268E-09	0.21669979E-09	0.23106290E-09	0.0	0.0	0.0	0.0
7.0	0.24331792E-09	0.24915647E-09	0.252510816E-09	0.0	0.0	0.0	0.0
7.2	0.2562835E-09	0.26914204E-09	0.25152835E-09	0.0	0.0	0.0	0.0
7.4	0.26602365E-09	0.25232472E-09	0.26760749E-09	0.0	0.0	0.0	0.0
7.6	0.2532299E-09	0.25684610E-09	0.26544833E-09	0.0	0.0	0.0	0.0
7.8	0.25675551E-09	0.25471003E-09	0.23553003E-09	0.0	0.0	0.0	0.0
8.0	0.19999558E-09	0.19380260E-09	0.17823466E-09	0.0	0.0	0.0	0.0
8.2	0.16021958E-09	0.13068303E-09	0.12636439E-09	0.0	0.0	0.0	0.0
8.4	0.11349927E-09	0.10681582E-09	0.8987230E-09	0.0	0.0	0.0	0.0
8.6	0.47139721E-10	0.45278853E-10	0.66873493E-10	0.0	0.0	0.0	0.0
8.8	0.6329408E-10	0.63634758E-10	0.57725991E-10	0.0	0.0	0.0	0.0
9.0	0.54146544E-10	0.51224025E-10	0.49203461E-10	0.0	0.0	0.0	0.0
9.2	0.46192189E-10	0.44714926E-10	0.46241850E-10	0.0	0.0	0.0	0.0



7d-65 RESPONSE FUNCTION VARIANCE, TWO INCH COLLIMATOR

0.0 0.20434667E-09 0.20181674E-09 0.19219440E-09  
0.18036778E-09 0.16456028E-09 0.15768950E-09 0.16141423E-09  
0.15646435E-09 0.13649632E-09 0.17108378E-09 0.17108378E-09  
0.16417243E-09 0.22017056E-09 0.20046732E-09 0.21036059E-09  
0.21762550E-09 0.220166479E-09 0.24224245E-09 0.23128532E-09  
0.22093172E-09 0.221434223E-09 0.20090769E-09 0.18352755E-09  
0.17275627E-09 0.16276272E-09 0.16622703E-09 0.16023406E-09  
0.16280635E-09 0.1575756E-09 0.16579016E-09 0.17428000E-09  
0.17591315E-09 0.17807526E-09 0.17654238E-09 0.17974214E-09  
0.17674427E-09 0.17531557E-09 0.17787016E-09 0.17656092E-09  
0.17740016E-09 0.17507269E-09 0.18534975E-09 0.18316229E-09  
0.16066435E-09 0.18113001E-09 0.18537297E-09 0.19100868E-09  
0.19261238E-09 0.1921511E-09 0.1917642E-09 0.19523363E-09  
0.19456065E-09 0.19779839E-09 0.20063026E-09 0.19962544E-09  
0.20355766E-09 0.20495047E-09 0.20396880E-09 0.19892911E-09  
0.20241639E-09 0.2045101E-09 0.22013705E-09 0.19643367E-09  
0.20182024E-09 0.19168393E-09 0.18294426E-09 0.1845331E-09  
0.17802971E-09 0.17111059E-09 0.18054665E-09 0.18439637E-09  
0.18151238E-09 0.17628571E-09 0.17945052E-09 0.18418042E-09  
0.17905077E-09 0.17402156E-09 0.1755136E-09 0.17760395E-09  
0.17651183E-09 0.17475146E-09 0.17542512E-09 0.17655039E-09  
0.16834971E-09 0.16091476E-09 0.16545609E-09 0.16789752E-09  
0.16534808E-09 0.16892709E-09 0.15976660E-09 0.15603482E-09  
0.15367049E-09 0.15501946E-09 0.15687013E-09 0.15570876E-09  
0.15276959E-09 0.15643054E-09 0.15921106E-09 0.15138840E-09  
0.15016591E-09 0.14902179E-09 0.14873110E-09 0.14825313E-09  
0.14531309E-09 0.14555201E-09 0.14702467E-09 0.14463774E-09  
0.13864933E-09 0.13980333E-09 0.1430794E-09 0.13836143E-09  
0.13601771E-09 0.13792177E-09 0.13984440E-09 0.13251278E-09  
0.13569654E-09 0.13803508E-09 0.13713612E-09 0.13416944E-09  
0.13799396E-09 0.1459559E-09 0.14706321E-09 0.14769746E-09  
0.14679464E-09 0.14553465E-09 0.14562164E-09 0.14706837E-09  
0.1465629E-09 0.14538656E-09 0.14597292E-09 0.15397135E-09  
0.15692037E-09 0.16443906E-09 0.17127816E-09 0.17283566E-09  
0.18672530E-09 0.19622827E-09 0.19525514E-09 0.20672029E-09  
0.22137285E-09 0.23120783E-09 0.2380977E-09 0.23523381E-09  
0.24190827E-09 0.2416911E-09 0.24356785E-09 0.24419666E-09  
0.23668626E-09 0.22887410E-09 0.222106043E-09 0.20989561E-09  
0.232875680E-09 0.17756647E-09 0.18751400E-09 0.18602009E-09  
0.16341615E-09 0.17074139E-09 0.16778542E-09 0.16807195E-09  
0.16141606E-09 0.15985026E-09 0.15851094E-09 0.15691697E-09  
0.15467011E-09 0.15333126E-09 0.15900544E-09 0.15343152E-09  
0.15304805E-09 0.15152199E-09 0.15348911E-09 0.15904669E-09  
0.15629180E-09 0.14942500E-09 0.1557730E-09 0.15115198E-09  
0.1581812E-09 0.15670291E-09 0.15530498E-09 0.16192499E-09  
0.1717361E-09 0.16262406E-09 0.162799406E-09 0.17384949E-09  
0.1711124E-09 0.17113559E-09 0.17998147E-09 0.17931819E-09  
0.16916187E-09 0.16973746E-09 0.16603678E-09 0.17833142E-09  
0.1808627E-09 0.17532761E-09 0.16640703E-09 0.16443320E-09  
0.17294959E-09 0.17438388E-09 0.17557640E-09 0.18486924E-09

0.18861102E-09 0.17695706E-09 0.18e28210E-09 0.17260480E-09  
0.18774760E-09 0.18344108E-09 0.18536253E-09 0.18951593E-09  
0.19327966E-09 0.18774760E-09 0.18536876E-09 0.197542E-09  
0.2033724E-09 0.20366937E-09 0.1828044E-09 0.19930177E-09  
0.19321219E-09 0.19473796E-09 0.20032964E-09 0.20919261E-09  
0.21237160E-09 0.2181000E-09 0.20707322E-09 0.21579045E-09  
0.22054666E-09 0.22549421E-09 0.23075739E-09 0.22194365E-09  
0.22875626E-09 0.23067515E-09 0.22907146E-09 0.23956632E-09  
0.23010185E-09 0.234975139E-09 0.235642847E-09 0.23956632E-09  
0.24353697E-09 0.24292689E-09 0.23421103E-09 0.23575700E-09  
0.252561750E-09 0.23026381E-09 0.21622363E-09 0.2162471E-09  
0.20361927E-09 0.19905516E-09 0.19827380E-09 0.19215526E-09  
0.16644806E-09 0.16143151E-09 0.15300229E-09 0.1364365E-09  
0.13364004E-09 0.1239478E-09 0.11356447E-09 0.11127148E-09  
0.97492139E-10 0.90980935E-10 0.79070972E-10 0.7376701E-10  
0.71308797E-10 0.70436101E-10 0.64515014E-10 0.63569284E-10  
0.58141681E-10 0.55266549E-10 0.50965928E-10 0.47420942E-10  
0.47142845E-10 0.44516016E-10 0.43842963E-10 0.42064267E-10  
0.41611992E-10 0.43215639E-10 0.37391627E-10 0.45006437E-10  
0.39597144E-10 0.37376796E-10 0.35732028E-10 0.35156378E-10  
0.37253450E-10 0.33422623E-10 0.35038167E-10 0.3535047E-10  
0.37538667E-10 0.39802772E-10 0.40748502E-10 0.40912954E-10  
0.42763321E-10 0.44613674E-10 0.52570652E-10 0.6117353E-10  
0.74383513E-10 0.79605541E-10 0.11192479E-09 0.14720450E-09  
0.19580657E-09 0.23618485E-09 0.31842176E-09 0.43059248E-09  
0.54013349E-09 0.67839086E-09 0.89145091E-09 0.11407943E-08  
0.1382723E-08 0.16631845E-08 0.21721143E-08 0.25769564E-08  
0.29223797E-08 0.33900127E-08 0.35611793E-08 0.39440913E-08  
0.4615456E-08 0.47806781E-08 0.50732503E-08 0.5135727E-08  
0.52546270E-08 0.54228018E-08 0.54947549E-08 0.52726223E-08  
0.50652744E-08 0.48960729E-08 0.46697501E-08 0.43954138E-08  
0.39065959E-08 0.36138297E-08 0.32283414E-08 0.27582769E-08  
0.2397379E-08 0.2230297E-08 0.19019008E-08 0.15414541E-08  
0.13223729E-08 0.11579391E-08 0.8618734E-09 0.64671335E-09  
0.51710747E-09 0.47807046E-09 0.37697512E-09 0.30695607E-09  
0.22631685E-09 0.17106523E-09 0.14387400E-09 0.12594624E-09  
0.83306209E-10 0.64144935E-10 0.52451890E-10 0.41949078E-10  
0.32524072E-10 0.26562583E-10 0.2207536E-10 0.18030494E-10  
0.14391477E-10 0.1192495E-10 0.10480105E-10 0.8624627E-11  
0.62311412E-11 0.66355029E-11 0.7156319E-11 0.62631744E-11  
0.3968822E-11 0.53248551E-11 0.43707581E-11 0.37863014E-11  
0.46566822E-11 0.49393632E-11 0.4320218E-11 0.40056291E-11  
0.33845756E-11 0.35798073E-11 0.34125220E-11 0.35044673E-11  
0.31866914E-11 0.24625944E-11 0.25082349E-11 0.3412421E-11  
0.35111640E-11 0.20937191E-11 0.33074750E-11 0.28628181E-11  
0.30016862E-11 0.35362000E-11 0.3789077E-11 0.34221584E-11  
0.31095924E-11 0.32380877E-11 0.34128421E-11 0.29194182E-11

























SR-95	RESPONSE	FUNCTION: HALF-INCH COLLIMATOR	0.0	0.0	0.33464721E-06	0.41070331E-06	0.47535131E-08
0.0	0.27835295E-05	0.27835295E-05	0.0	0.0	0.14367475E-06	0.54760454E-06	0.513337942L-07
0.27864219E-05	0.35178955E-05	0.41678195E-05	0.0	0.76056139E-08	0.95070241E-09	0.0	0.85563215E-07
0.26523976E-05	0.27375602E-05	0.32884163E-05	0.0	0.0	0.0	0.16732355E-06	0.0
0.15696096E-05	0.11229577E-05	0.24484725E-05	0.0	0.0	0.0	0.0	0.0
0.22619597E-05	0.21627275E-05	0.22619955E-05	0.0	0.0	0.0	0.0	0.0
0.13509480E-05	0.23144230E-05	0.16218974E-05	0.0	0.0	0.0	0.0	0.0
0.33768338E-05	0.32580547E-05	0.21951691E-05	0.0	0.0	0.0	0.0	0.0
0.23006960E-05	0.32552434E-05	0.26442654E-05	0.0	0.0	0.0	0.0	0.0
0.14707357E-05	0.28834766E-05	0.36430911E-05	0.0	0.0	0.0	0.0	0.0
0.17055970E-05	0.23292178E-05	0.29043931E-05	0.0	0.0	0.0	0.0	0.0
0.19907720E-05	0.22455561E-05	0.24241090E-05	0.0	0.0	0.0	0.0	0.0
0.22596405E-05	0.32190703E-05	0.33702381E-05	0.0	0.0	0.0	0.0	0.0
0.18890460E-05	0.19447198E-05	0.22088337E-05	0.0	0.0	0.0	0.0	0.0
0.30584097E-05	0.27185507E-05	0.21340902E-05	0.0	0.0	0.0	0.0	0.0
0.36202728E-05	0.17008051E-05	0.26315411E-05	0.0	0.0	0.0	0.0	0.0
0.21514397E-05	0.26610160E-05	0.28108315E-05	0.0	0.0	0.0	0.0	0.0
0.36202728E-05	0.27142542E-05	0.30137239E-05	0.0	0.0	0.0	0.0	0.0
0.18995024E-05	0.1793624E-05	0.16276026E-05	0.0	0.0	0.0	0.0	0.0
0.31087966E-05	0.34272825E-05	0.32181279E-05	0.0	0.0	0.0	0.0	0.0
0.32361922E-05	0.31268564E-05	0.31601357E-05	0.0	0.0	0.0	0.0	0.0
0.40319264E-05	0.35280564E-05	0.35052397E-05	0.0	0.0	0.0	0.0	0.0
0.32523694E-05	0.37657337E-05	0.47002723E-05	0.0	0.0	0.0	0.0	0.0
0.37495711E-05	0.32348844E-05	0.37704831E-05	0.0	0.0	0.0	0.0	0.0
0.34833711E-05	0.25116481E-05	0.1926729E-05	0.0	0.0	0.0	0.0	0.0
0.18861929E-05	0.12330611E-05	0.11969341E-05	0.0	0.0	0.0	0.0	0.0
0.11979437E-05	0.10429023E-05	0.94975206E-06	0.0	0.0	0.0	0.0	0.0
0.37552741E-06	0.0	0.13081662E-05	0.0	0.0	0.0	0.0	0.0
0.63687222E-06	0.69116038E-06	0.11560542E-05	0.0	0.0	0.0	0.0	0.0
0.10324629E-05	0.93454048E-06	0.38028082E-06	0.0	0.0	0.0	0.0	0.0
0.78623100E-06	0.11712655E-05	0.30442473E-07	0.0	0.0	0.0	0.0	0.0
0.63506357E-06	0.65978770E-06	0.34985834E-06	0.0	0.0	0.0	0.0	0.0
0.79096436E-06	0.10495760E-05	0.66644202E-06	0.0	0.0	0.0	0.0	0.0
0.13347862E-05	0.17492930E-05	0.25706968E-05	0.0	0.0	0.0	0.0	0.0
0.57954767E-05	0.76702672E-05	0.93244862E-05	0.0	0.0	0.0	0.0	0.0
0.16930106E-04	0.21768225E-04	0.26171881E-04	0.0	0.0	0.0	0.0	0.0
0.44844594E-04	0.48980190E-04	0.54973381E-04	0.0	0.0	0.0	0.0	0.0
0.63430838E-04	0.64313150E-04	0.66731678E-04	0.0	0.0	0.0	0.0	0.0
0.6072380F-04	0.55688375E-04	0.52357078E-04	0.0	0.0	0.0	0.0	0.0
0.40180802E-04	0.28201612E-04	0.21310949E-04	0.0	0.0	0.0	0.0	0.0
0.14268141E-04	0.11968391E-04	0.87464614E-05	0.0	0.0	0.0	0.0	0.0
0.48866104E-05	0.30840793E-05	0.16580234E-05	0.0	0.0	0.0	0.0	0.0
0.89746317E-06	0.58373138E-06	0.36126653E-06	0.0	0.0	0.0	0.0	0.0
0.57602725E-06	0.0	0.30978810E-07	0.0	0.0	0.0	0.0	0.0
0.15211231E-06	0.15211238E-07	0.0	0.0	0.0	0.0	0.0	0.0
0.10647858E-06	0.0	0.0	0.0	0.0	0.0	0.0	0.0
0.38028094E-07	0.0	0.0	0.0	0.0	0.0	0.0	0.0
0.0	0.74154741E-07	0.30422473E-07	0.0	0.0	0.0	0.0	0.0
0.56091448E-07	0.0	0.13690101E-06	0.0	0.0	0.0	0.0	0.0
0.11173217E-06	0.84612566E-07	0.16732355E-06	0.0	0.0	0.0	0.0	0.0
0.12359127E-07	0.26524572E-06	0.45633698E-07	0.0	0.0	0.0	0.0	0.0

















ZN-05 RESPONSE FUNCTION VARIANCE HALF-PIGCH COLLIMATOR

0.0 0.10757098E-11 0.73571493E-12 0.57840050E-12  
0.50558955E-12 0.45615380E-12 0.42238917E-12 0.39110428E-12  
0.35960492E-12 0.33182804E-12 0.34359686E-12 0.42928866E-12  
0.49726389E-12 0.47569679E-12 0.42223786E-12 0.39166570E-12  
0.38298970E-12 0.39117180E-12 0.36791772E-12 0.36514932E-12  
0.35068194E-12 0.34503044E-12 0.31499613E-12 0.28864616E-12  
0.26503729E-12 0.25317107E-12 0.24711689E-12 0.26712356E-12  
0.26799461E-12 0.27532788E-12 0.28427721E-12 0.28877530E-12  
0.28426588E-12 0.28359097E-12 0.29421394E-12 0.30252530E-12  
0.29548715E-12 0.29418050E-12 0.29215172E-12 0.28743085E-12  
0.28610462E-12 0.31130025E-12 0.27075413E-12 0.29279725E-12  
0.28482886E-12 0.30064177E-12 0.29966127E-12 0.29478476E-12  
0.29167272E-12 0.30636397E-12 0.31310436E-12 0.31630462E-12  
0.31056135E-12 0.30161057E-12 0.30638084E-12 0.29619434E-12  
0.29310756E-12 0.29220921E-12 0.28939185E-12 0.27657480E-12  
0.28333064E-12 0.28331661E-12 0.26873962E-12 0.25093560E-12  
0.25644070E-12 0.25729843E-12 0.26610935E-12 0.27086916E-12  
0.26508700E-12 0.24688931E-12 0.25999710E-12 0.26131777E-12  
0.25801675E-12 0.24497255E-12 0.25055235E-12 0.23945370E-12  
0.22652995E-12 0.22401016E-12 0.21444429E-12 0.20938633E-12  
0.20212436E-12 0.19432396E-12 0.19244507E-12 0.18229727E-12  
0.19133905E-12 0.17255425E-12 0.18078924E-12 0.17017968E-12  
0.16546367E-12 0.16562359E-12 0.16439090E-12 0.16347129E-12  
0.16660181E-12 0.16750896E-12 0.16893388E-12 0.15460369E-12  
0.15184338E-12 0.15365357E-12 0.15454318E-12 0.15841332E-12  
0.15178365E-12 0.14774434E-12 0.14287768E-12 0.14361234E-12  
0.14679354E-12 0.13497661E-12 0.13427313E-12 0.13490213E-12  
0.12983348E-12 0.12192195E-12 0.12985489E-12 0.13245308E-12  
0.12726734E-12 0.12167703E-12 0.12936505E-12 0.12696924E-12  
0.11797150E-12 0.11517100E-12 0.11439326E-12 0.11695977E-12  
0.12481818E-12 0.11845061E-12 0.12564889E-12 0.11567367E-12  
0.12346487E-12 0.11074133E-12 0.11306266E-12 0.10944219E-12  
0.96110674E-13 0.10306388E-12 0.99379957E-13 0.92753333E-13  
0.89004921E-13 0.88815077E-13 0.84529822E-13 0.86036213E-13  
0.74162898E-13 0.68842447E-13 0.63878048E-13 0.60666424E-13  
0.58331161E-13 0.52373568E-13 0.49801004E-13 0.50998759E-13  
0.50644755E-13 0.46330127E-13 0.43396029E-13 0.41310962E-13  
0.45674659E-13 0.47688914E-13 0.46943542E-13 0.52780737E-13  
0.52043076E-13 0.52002300E-13 0.52291187E-13 0.62329639E-13  
0.62477385E-13 0.65824353E-13 0.70239170E-13 0.70197212E-13  
0.66874186E-13 0.65386119E-13 0.70947588E-13 0.74688589E-13  
0.75880454E-13 0.76898120E-13 0.75357309E-13 0.83993034E-13  
0.76356318E-13 0.70874404E-13 0.71492020E-13 0.74910022E-13  
0.77212600E-13 0.7801997E-13 0.76081997E-13 0.80202229E-13  
0.75676824E-13 0.77891699E-13 0.76411533E-13 0.72343942E-13  
0.68936447E-13 0.67307325E-13 0.72514206E-13 0.70033172E-13  
0.64634604E-13 0.63799537E-13 0.65441901E-13 0.67062350E-13  
0.62845671E-13 0.55200273E-13 0.59704357E-13 0.53613736E-13  
0.56723453E-13 0.52133984E-13 0.60311402E-13 0.56339566E-13  
0.50033900E-13 0.47269182E-13 0.50666418E-13 0.51128704E-13

0.50064539E-13 0.49407642E-13 0.50142382E-13 0.50174359E-13  
0.45489118E-13 0.50451149E-13 0.48172702E-13 0.45478507E-13  
0.44046983E-13 0.46211349E-13 0.46554601E-13 0.44683545E-13  
0.51008429E-13 0.46659657E-13 0.49935637E-13 0.47031961E-13  
0.47281318E-13 0.45915095E-13 0.44978059E-13 0.50259476E-13  
0.45403927E-13 0.44328531E-13 0.46010894E-13 0.46351679E-13  
0.45265339E-13 0.48310863E-13 0.49588704E-13 0.48661696E-13  
0.41762265E-13 0.42119212E-13 0.45212288E-13 0.46692380E-13  
0.44850262E-13 0.47107598E-13 0.46277130E-13 0.44245622E-13  
0.41421524E-13 0.44044954E-13 0.43487275E-13 0.43677957E-13  
0.41039588E-13 0.45947041E-13 0.45137762E-13 0.46234701E-13  
0.48140728E-13 0.42284041E-13 0.39834960E-13 0.39824304E-13  
0.41847656E-13 0.41740746E-13 0.36459476E-13 0.39185408E-13  
0.36757618E-13 0.36499515E-13 0.38154531E-13 0.36715016E-13  
0.34116878E-13 0.34926126E-13 0.35914535E-13 0.33360840E-13  
0.32674408E-13 0.32527386E-13 0.31249177E-13 0.33426410E-13  
0.32404933E-13 0.32423801E-13 0.32024845E-13 0.32785231E-13  
0.33467325E-13 0.35192349E-13 0.31838129E-13 0.30049239E-13  
0.3105287E-13 0.31465468E-13 0.28526282E-13 0.28079332E-13  
0.29612668E-13 0.30155708E-13 0.26703848E-13 0.28963130E-13  
0.32711405E-13 0.27064199E-13 0.31401588E-13 0.29239971E-13  
0.31689075E-13 0.253895420E-13 0.30496652E-13 0.28117651E-13  
0.30155708E-13 0.24022349E-13 0.25917721E-13 0.29325165E-13  
0.31689075E-13 0.26684397E-13 0.27781176E-13 0.31529339E-13  
0.32743221E-13 0.31736100E-13 0.36555306E-13 0.43955796E-13  
0.39185408E-13 0.46724266E-13 0.52026306E-13 0.55945694E-13  
0.57074300E-13 0.68148503E-13 0.78029422E-13 0.86665759E-13  
0.98849567E-13 0.10556615E-12 0.11418053E-12 0.12986941E-12  
0.13850124E-12 0.14946876E-12 0.15520826E-12 0.14011903E-12  
0.1522051E-12 0.16236483E-12 0.16648472E-12 0.16389716E-12  
0.13340083E-12 0.12692852E-12 0.14413405E-12 0.13633411E-12  
0.12011177E-12 0.11187004E-12 0.10085946E-12 0.95574276E-13  
0.79563363E-13 0.74281835E-13 0.65454476E-13 0.56710277E-13  
0.50291497E-13 0.47377444E-13 0.42783217E-13 0.36459476E-13  
0.32540926E-13 0.32098026E-13 0.25044576E-13 0.29403874E-13  
0.26019551E-13 0.24139470E-13 0.22489026E-13 0.24142742E-13  
0.22829727E-13 0.22925570E-13 0.22116305E-13 0.19688519E-13  
0.20646865E-13 0.19188064E-13 0.16302409E-13 0.15801942E-13  
0.16366289E-13 0.17047492E-13 0.18836666E-13 0.16366289E-13  
0.14636631E-13 0.13459340E-13 0.17037136E-13 0.14311873E-13  
0.14526030E-13 0.21296404E-13 0.17636088E-13 0.14651435E-13  
0.14875549E-13 0.15397304E-13 0.15610255E-13 0.16217181E-13  
0.17889733E-13 0.16313048E-13 0.14681960E-13 0.18155104E-13  
0.20614932E-13 0.17995456E-13 0.13523240E-13 0.14111873E-13  
0.19251961E-13 0.16941293E-13 0.16696395E-13 0.15855183E-13  
0.15631563E-13 0.15929718E-13 0.15119785E-13 0.16076789E-13  
0.18740838E-13 0.144801560E-13 0.20274174E-13 0.19397326E-13  
0.20540383E-13 0.18400110E-13 0.22318617E-13 0.20137951E-13  
0.20785311E-13 0.21807541E-13 0.20732039E-13 0.19422310E-13  
0.20274174E-13 0.22829272E-13 0.20242210E-13 0.24022347E-13



EXPERIMENTAL DETERMINATION OF GAMMA-RAY RESPONSE  
FUNCTIONS FOR THE KSU SPECTROMETER SYSTEM

by

ROGER S. REYNOLDS

B. S., University of Nevada, 1965

---

AN ABSTRACT OF  
A MASTER'S THESIS

submitted in partial fulfillment of the  
requirements for the degree

MASTER OF SCIENCE

Department of Nuclear Engineering

KANSAS STATE UNIVERSITY  
Manhattan, Kansas

1969

## ABSTRACT

Using a collimated sodium iodide scintillator with associated electronics and a multichannel pulse-height analyzer, pulse-height spectra were measured for the collimator viewing monoenergetic plane sources of gamma radiation. These "response functions" (ratios of the counts per pulse-height unit per unit time to differential gamma-ray flux per steradian at the source plane) were measured for nine gamma-ray energies between 46 keV and 1.114 MeV, and for two collimator aperture sizes (two-inch diameter and one-half inch diameter). A point source superposition technique was used to simulate the infinite plane source.

The two-inch collimator response functions were compared with previously measured responses on the same system. The two measurements were made independently of each other and used two different techniques for simulating the infinite plane source. The response functions agreed favorably. No such direct comparison was possible with the half-inch collimator response functions since no previous data were available.

The source strengths of the point sources were determined using three different methods. An absolute counting technique was used for four of the calibrations; comparative counting was used for two of the determinations. National Bureau of Standards certified sources were used for the comparative method. Three of the determinations were based on intercomparisons of data with data from the other six measurements.



